0

Università degli Studi di Salerno

Dipartimento di Ingegneria Industriale

Electronic Engineering Master's thesis

Control design for a voltage regulator in a single-phase grid-connected PV inverter

Candidato: Gallo Antonio
Matricola: 0622400425

Relatore: Heinrich Christoph Neizert
Correlatore: Domingo Biel Sole

ANNO ACCADEMICO 2018–2019

Abstract

This work presents the design guidelines of a control for direct regulation of the voltage amplitude at the connection point of a single-phase grid-connected PV inverter. The parameters of such control are designed for ensuring locally asymptotic stability for a given range of the impedance. Usually, the design of the controllers are done by applying the drop method approximation. This work evaluates the application of another method, that consists in a linearization of the non-linear curve relating the amplitude of the voltage at the connection point with the injected active and reactive power. It has been studied the control strategy of drop method and new control strategy, which considers the real function and its linearization. Numerical simulations for the last method confirm the expected proper voltage regulation and the control robustness with respect to the grid impedance variations without the requirement of any estimation or measure of the actual impedance.
This thesis shows, through a comparison between the drop method and the linearization method, what is the more realistic one. The results show that the linearization method is faster and has more accuracy than the drop method. This is more evident when one or more control parameters change.

Contents

Chapter 1

Introduction

The penetration of photovoltaic (PV) systems in the electricity network has been increased in the last decades. When operating with a low voltage (LV) network the PV installation produce an undesirable phenomenon of voltage fluctuation in the connection point. This problem is specially serious when the network has a high R/X ratio, as usually happens in LV networks. Moreover, this effect is compounded by the injected active power.

In grid-connected PV inverters the voltage is usually controlled by regulating the reactive power delivered to the grid. In the literature one can find several techniques devoted to design such control [1], [2], [3], [4]. Most of them are based on the droop control method. The regulation of the delivered reactive power and the active power is achieved by the design of two different control loops. The inner one is a current loop in charge to ensure the injection of the grid current that provides the desired active and reactive power. On the other hand, the outer loop regulates the powers and generates the reference current for the inner one. The inner loop controller can be designed by using linear control techniques in a rotating frame dq [5], [6], [7] or in a time-variant framework [8], [9], [10], [11], [12], [13] or applying nonlinear control techniques as Lyapunov-based control [14] or passivity-based control [15].

The outer loop design assumes that the internal PV inverter variables reached their steady-state regime, although this assumption the dynamical description of the complete system is highly nonlinear and the controllers design is even worsened by the unknown impedance that exists between the connection point and the grid source. In order to overcome the aforementioned problems, the droop control method uses an approximation of the voltage fluctuation depending on the resistive and the reactive parts of the grid impedance and evaluates the impact of the grid impedance variation in the control design. Alternatively, this work develops a rigorous mathematical description of the nonlinear dynamics of the grid-connected PV inverter,

applies a linearization procedure and designs PI controllers to ensure closed-loop asymptotic stability and the desired voltage regulation. Variations of the grid impedance and the active power delivered to the grid are included in the analysis, thus ensuring the proper power regulation over the whole working range without any measure or estimation of the grid impedance.
This elaborate of thesis was done at the Universitad Politecnica de Catalunya (UPC), in the control system laboratory with the professor Domingo Biel Sole. In the following chapters are described the problems for the control design of a PV inverter when is connected to a weakly grid.
In the second chapter is introduced the problem statement, i.e. the problems for a weakly grid and the differences that are present between a ideal-grid (strong grid) and non-ideal grid (weakly grid). In this chapter is present also discussed the passivity based control, used for the inner loop of the system for regulation of the reference current. At the end of the chapter, using Matlab-Simulink, some simulations are presented, which show the variations of voltage amplitude, the current amplitude and the phase shift changing the values of active and reactive power injected.
In the third chapter is discussed about the closed-loop system modelling. It has been shown how to simplify and to linearize the generical model of the PV inverter and it has been demostrated as the MPPT control is not good for the application of the subject. The final control scheme has been shown at the end of the chapter and is used for the outer loop (power regulator). This is composed by two PI controllers used to regulate the voltage amplitude at connection point.
In the fourth chapter the Drop method is explained and its use in this subject. In the chapter are shown the equations and the control scheme used for the Drop method and the simulations of a weakly grid controlled using the Drop method for few combination of parameters.
In the fifth chapter the Linearization method is explained, that is an alternative method more efficient than the last one. Also here, are shown the equations used and the control scheme. Finally, are introduced the simulations in the same conditions used for the Drop method.
In the sixth the methods presented in the previous chapters are compared with the real behavior and will be seen what of the two methods has a trend closer to the real one. This comparison has been done using Matlab-Simulink simulations, i.e. are shown the root locus graph of the closed loop system, the voltage amplitude at connection point curve and the active and reactive power curves.
Finally, the last chapter summarizes the conclusions of the thesis work.

Chapter 2

Problem statement

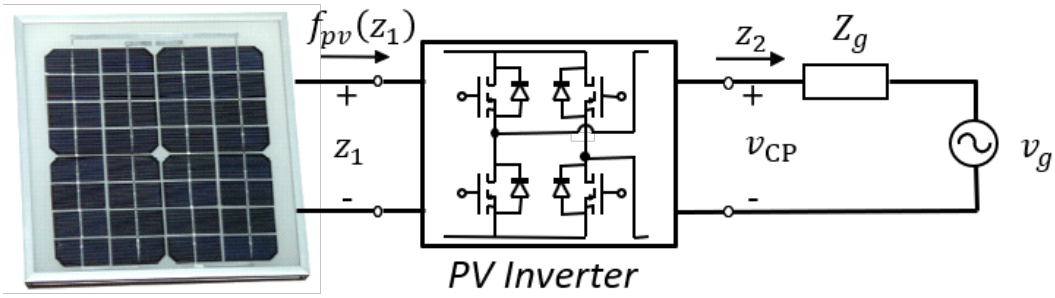

Figure 2.1: PV inverter connected to a non-ideal grid.

Fig. 2.1 shows the circuit scheme of a PV inverter connected to a non-ideal grid, where the non-ideal grid is modelled by an impedance, Z_g, in series with an ideal sinusoidal voltage source, v_g. The state equations (in averaged values) of the PV inverter are:

$$C\dot{z}_1 = -uz_2 + f_{pv}(z_1), \tag{2.1a}$$
$$L\dot{z}_2 = uz_1 - v_{CP}, \tag{2.1b}$$

where z_1 and z_2 correspond to the capacitor voltage and the inductor current, respectively, L is the inductance, C is the capacitance, $u \in [-1, 1]$ is the control and $f_{pv}(z_1) = \Lambda - \Psi e^{(\alpha z_1)}$ is the current delivered by the PV array. The parameters L and C are assumed to be known constants.

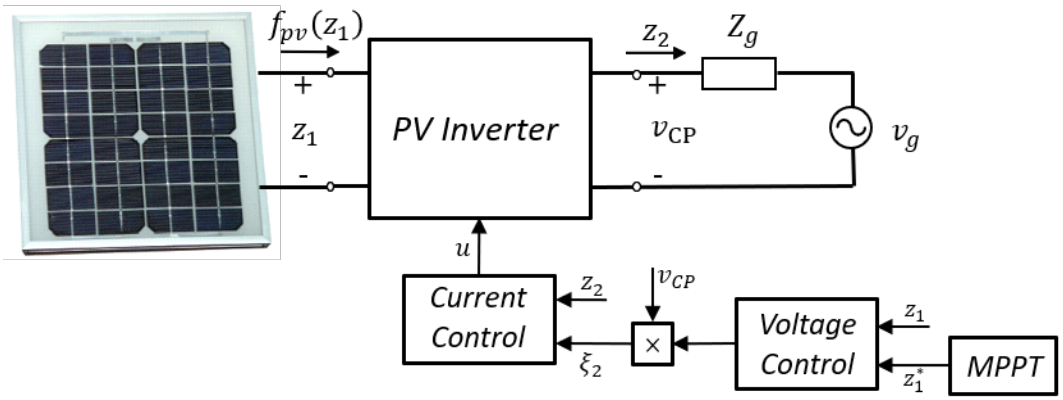

Figure 2.2: Power control for a PV inverter connected to a non-ideal grid

The PV inverter has to be controlled in order to perform two main tasks:

- To provide the desired active power to the grid (the active power reference value could be given by a Maximum Power Point Tracker (**MPPT**), for instance).

- To regulate the amplitude of the voltage at the connection point to the value of the amplitude of the ideal grid voltage. This is possible by an injected reactive power control which provides the reference value of reactive power to the grid.

When the voltage at the connection point is $v_{cp} = A_{cp}\sin(\omega t)$ and the injected current is given by $z_2 = A_I \sin(\omega t - \theta)$, the PV inverter injects an active power, $P = \frac{A_{cp}A_I}{2}\cos\theta$, and a reactive power, $Q = \frac{A_{cp}A_I}{2}\sin\theta$.

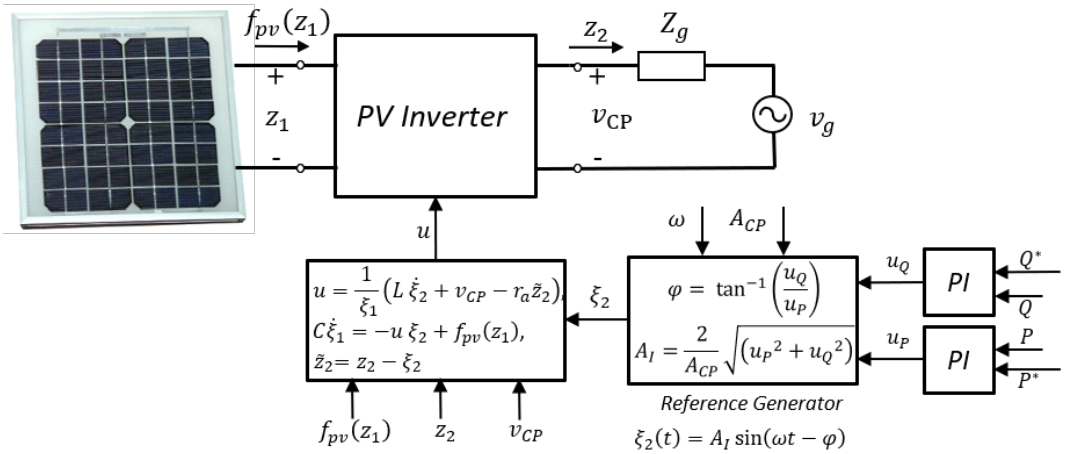

Figure 2.3: Control scheme of a PV inverter connected to a non-ideal grid (extract from [15]).

Fig. 2.3 presents the block diagram of a control system that could perform the previously mentioned control specifications. In this document will be used for the system a passivity-based control, a Q-control and a P-control. The research of the proper dynamical models allows to design the parameters of the controllers. Obviously, the passivity-based control is only one of the methods in the literature, but for the purpose of this document it will be used it, recalling the paper [15].

2.1 Current control: Passivity-based control

As reported in the paper [15], where has been discussed and explained the Passivity based control in depth, in my document I have summarized for the subject in question.
The proposed control ensures that the PV inverter tracks the reference current guaranteeing stability of the overall system written in terms of the error variables. Consider the system defined before, where C and L are known constant parameters. A nonlinear dynamic feedback passivity-based controller is given by:

$$u = \frac{1}{\zeta_1}\left(L\dot{\zeta}_2 + v_{CP} - r_a(z_2 - \zeta_2)\right) \tag{2.2a}$$

$$C\dot{\zeta}_1 = -u\zeta_2 + f_{pv}(z_1) \tag{2.2b}$$

The reference current being $\zeta_2 = A_I \sin(\omega t - \theta)$ and being the controller parameter $r_a > 0$. Under these conditions and assuming $\zeta_1(t) > 0$, the controller solves the tracking problem of the grid injected current

$$\lim_{t\to\infty} z_2(t) = \zeta_2(t)$$

Defining the variables $\tilde{z_1} = z_1 - \zeta_1$, $\tilde{z_2} = z_2 - \zeta_2$ the system equations can be rewritten as:

$$C\dot{\tilde{z_1}} = -u\tilde{z_2} - u\zeta_2 + f_{pv}(z_1) - u\dot{\zeta_1} \tag{2.3a}$$

$$L\dot{\tilde{z_2}} = u\tilde{z_1} + u\zeta_1 - v_{CP} - L\dot{\zeta_2} \tag{2.3b}$$

Replacing the controller equations, the following equations can be obtained:

$$C\dot{\tilde{z_1}} = -u\tilde{z_2} \tag{2.4a}$$

$$L\dot{\tilde{z_2}} = u\tilde{z_1} - r_a\tilde{z_2} \tag{2.4b}$$

In order to prove the stability of the system, consider the following lower bounded Lyapunov function:

$$V = \frac{1}{2}C{\tilde{z_1}}^2 + \frac{1}{2}L{\tilde{z_2}}^2 \tag{2.5}$$

where the time derivative along the trajectories of 2.4 are given by

$$\dot{V} = \tilde{z_1}(-u\tilde{z_2}) + \tilde{z_2}(u\tilde{z_1} - r_a\tilde{z_2}) = -r_a{\tilde{z_1}}^2 \leq 0 \tag{2.6}$$

which indicates that $\dot{V}$ is a negative semi-definite function and thus the variables $\tilde{z_1}$ and $\tilde{z_2}$ are also bounded. Furthermore, following Barbalat's lemma [25], the global asymptotic convergence of the tracking error $\tilde{z_1}$ to zero is guaranteed because the boundedness of u, $\tilde{z_1}$ and $\tilde{z_2}$ implies the boundedness of $\dot{\tilde{z_2}}$ and therefore the uniform continuity of $\dot{V}$. Notice that the boundedness of the control signal $u = \frac{1}{\zeta_1}(L\dot{\zeta_2} + v_{CP} - r_a\tilde{z_2})$ is ensured since all the involved variables are bounded and the controller variable $\tilde{z_1}$ is assumed bounded away from zero. Moreover, when the perfect tracking is achieved, $\tilde{z_2} = 0$, the error system simplifies in $\dot{\tilde{z_1}} = 0$ and $u\tilde{z_1} = 0$. Taking into account that the control signal u is a time variant signal the last expression implies that $\tilde{z_1} = 0$ and $\zeta_1 = z_1$. For what has just been said, it can be done some remarks:

- Numerical simulations show that ζ_1 converges quickly to z_1 when the value of $\zeta_1(0)$ is selected to be equal to the initial condition of the PV output voltage.
- The convergence rate of the Lyapunov function depends on the value of the control parameter r_a.
- When reference $\zeta_2(t) = A_I \sin(\omega t - \theta)$ is selected such that $A_I = \frac{2}{A_{CP}}\sqrt{(P^{*2} + Q^{*2})}$ and $\theta = \tan^{-1}(\frac{Q^*}{P^*})$, the PV inverter delivers the desired active, P^*, and reactive power, Q^*, to the grid.

2.2 Ideal Case (Strong Grid)

In this case, as shown in the Fig.2.3, the amplitude of the voltage at the connection point is fixed by the amplitude of the sinusoidal source. This because the output impedance has only a resistive part, so the reactive power to provide at the grid is nothing.
The existence or not of feedback of the active and reactive power will lead to an indirect control framework or a direct active and reactive power control.

Simulations In order to validate the control, the controlled system has been tested using Matlab-Simulink. For the simulation we consider the system of the Fig.2.3 with $C = 2.2mF$, $L = 950\mu H$, $v_g = 312\sin(100\pi t)V$ and a PV array with a peak power of $3.3kW$, a short circuit current of $6.1A$, and an open circuit voltage of $678V$ at $1000\frac{W}{m^2}$ ($\Lambda = 6.1$, $\alpha = 0.026$, $\Psi = 1.35 * 10^7$). The control parameter r_a is set to 1 and $\zeta_1(0) = 500V$. The initial condition of the capacitor voltage is of $500V$.
The following plots show the simulation results when the active power and the reactive power are regulated to $P^* = 2kW$ and $Q^* = -2kVAr$, respectively. In $t = 0.6s$ the references are changed to $P^* = 3kW$ and $Q^* = -1kVAr$.

The Fig.2.4 (left) shows the PV voltage, the PV current, (which has been amplified by 10 for a better view), the grid voltage and the injected current (amplified by 10). The PV inverter output current has a phase shift with respect to the grid, thus indicating the injection of reactive power.
The PV voltage decreases when the active power increases, the contrary happens with the PV current as it is usual in PV curves. On the other hand, the Fig.2.4 (right) pictures the PV power, the active power and the reactive power. Notice from the plot that the reference values are reached in just one grid period.

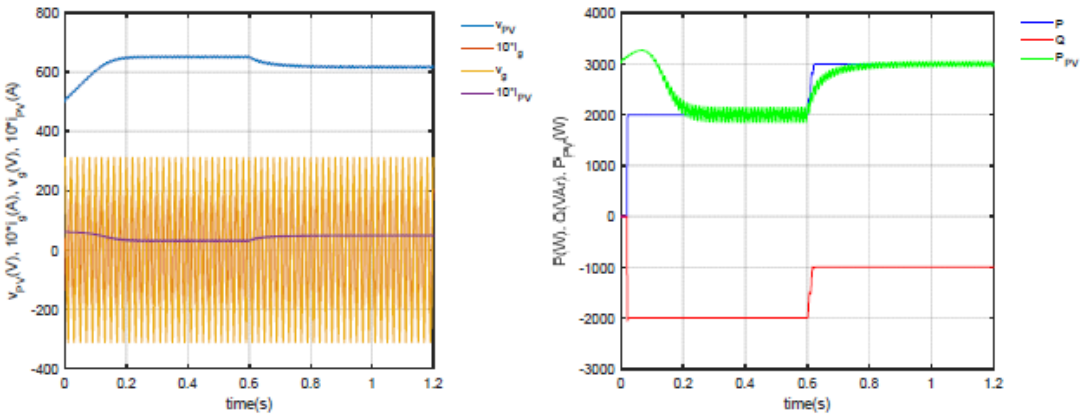

Figure 2.4: Left: PV voltage (V), PV current (A) (amplified by 10), grid voltage (V) and injected current (A) (amplified by 10); right: PV power (W), active power (W) and reactive power (VAr).

The control system has also been tested when an irradiance change is applied. The irradiance varies from the initial value of $1000\frac{W}{m^2}$ to $750\frac{W}{m^2}$.

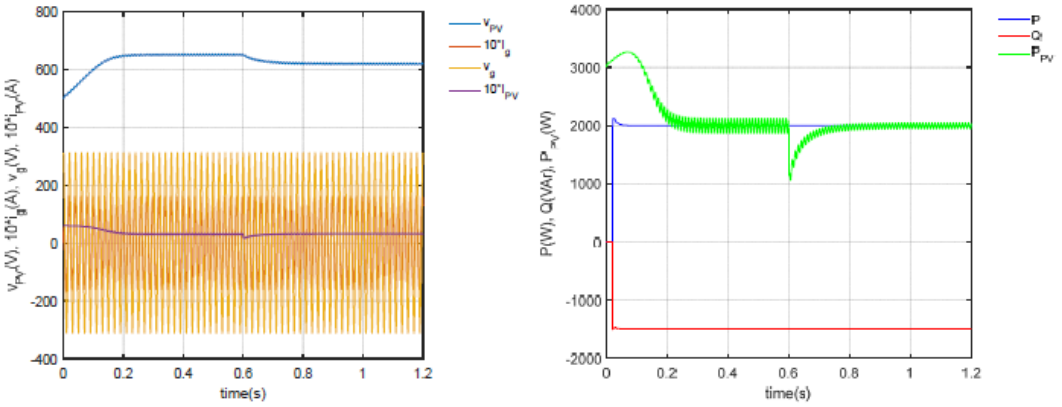

Figure 2.5: Left: PV voltage (V), PV current (A) (amplified by 10), grid voltage (V) and injected current (A) (amplified by 10); right: PV power (W), active power (W) and reactive power (VAr).

The Fig.2.5 and Fig.2.4 shows the simulation results. Notice how the active and the reactive power are properly regulated to their reference values to $P^* = 2kW$ and $Q^* = 1.5kVAr$, respectively, without any transient when the irradiance changes.

2.3 Non-ideal Case (Weak Grid)

In this case, the PV inverter has an impedance between the connection point and the ideal sinusoidal source. The amplitude of the voltage at the connection point will depends on the active and the reactive power injected to the grid. The relationship among those variables can be obtained as described in the following lines. The PV inverter output network equation is:

$$v_{CP} = v_{Z_g} + v_g \tag{2.7}$$

where:

- $v_{CP} = A_{CP}\sin(\omega t)$ is the voltage at CP,
- $v_{Z_g} = A_I|Z_g|\sin(\omega t - \theta + \theta_{Z_g})$ is the voltage through the impedance, A_I is the amplitude of the injected current and θ the phase shift between the voltage and the current at CP,
- $v_g = A\sin(\omega t + \phi)$ is the ideal grid voltage, being ϕ the phase shift between the grid source and the output voltage of the PV inverter.

Hence, the equation can be rewritten as:

$$A_{CP}\sin(\omega t) = A_I|Z_g|\sin(\omega t - \theta + \theta_{Z_g}) + A\sin(\omega t + \phi) \tag{2.8}$$

which, replacing the current amplitude expression $A_I = \frac{2}{A_{CP}}\sqrt{P^2+Q^2}$ and the phase shift expression $\theta = \tan^{-1}(\frac{Q}{P})$ in terms of the active and reactive power, results in:

$$A_{CP}\sin(\omega t) = \frac{2}{A_{CP}}\sqrt{P^2+Q^2}|Z_g|\sin(\omega t - \tan^{-1}(\frac{Q}{P}) + \theta_{Z_g}) + A\sin(\omega t + \phi) \tag{2.9}$$

Recalling the trigonometric property: $\sin(\alpha+\beta) = \sin\alpha\cos\beta + \sin\beta\sin\alpha$ and defining $\Gamma = 2\sqrt{(P^2+Q^2)}|Z_g|$ and $\psi = -\tan^{-1}(\frac{Q}{P}) + \theta_{Z_g}$ the equation becomes:

$$\begin{aligned} A_{CP}^2\sin(\omega t) = \Gamma(\sin(\omega t)\cos(\psi) + \cos(\omega t)\sin(\psi)) + \\ + A_{CP}A(\sin(\omega t)\cos(\phi) + \cos(\omega t)\sin(\phi)) \end{aligned} \tag{2.10}$$

or

$$\begin{aligned} A_{CP}^2\sin(\omega t) = (\Gamma\cos(\psi) + A_{CP}A\cos(\phi))\sin(\omega t) + \\ (\Gamma\sin(\psi) + A_{CP}A\sin(\phi))\cos(\omega t) \end{aligned} \tag{2.11}$$

and, recalling trigonometric properties, the following set of equations should be solved for A_{CP} and ϕ:

$$\Gamma\cos(\psi) + A_{CP}A\cos(\phi) = A_{CP}^2, \tag{2.12a}$$
$$\Gamma\sin(\psi) + A_{CP}A\sin(\phi) = 0. \tag{2.12b}$$

Finally, the following second order algebraic equation can be easily obtained:

$$x^2 - (A^2 + 2\Gamma\cos(\psi))x + \Gamma^2 = 0. \tag{2.13}$$

where the variable $x = A_{CP}^2$ has been defined, with the solutions:

$$x = \frac{A^2 + 2\Gamma\cos(\psi) \pm \sqrt{A^2 + 2\Gamma\cos(\psi)^2 - 4\Gamma^2}}{2} \tag{2.14}$$

Considering that $\Gamma \geq 0$, the two solutions of (2.13) are positive real when $|A^2 + 2\Gamma\cos(\psi)| \geq 2\Gamma$. Taking into account that both solutions provide the same active power, it is clear that the upper one is the proper one for the voltage regulation since it requires less injected current [15]. Once A_P is calculated, the amplitude of the injected current and the proper grid phase shift can be also determined by solving:

$$A_I = \frac{2}{A_{CP}}\sqrt{P^2 + Q^2} \tag{2.15}$$

and

$$\phi = \sin^{-1}(\frac{-\Gamma}{A_{CP}A}\sin(\psi)) \tag{2.16}$$

Simulation The Fig. 2.6 shows the amplitude values of the voltage at the connection point, A_{CP}, and the injected current, A_I, when the PV inverter supplies an active power $P = 2kW$ to a grid network with an equivalent impedance of a series inductance ($L_g = 2mH$) and a resistance of ($R_g = 2\Omega$). The reactive power varies from $-8kVAr$ to $8000kVAr$ in steps of $500VAr$. Notice that the voltage is increased following the reactive power trend and how the current amplitude has an expected minimum when the reactive power is zero. It is also clear that the solution to be controlled corresponds to the one close to the amplitude of the grid of $312V$ since the current amplitude is always lower than the one giving by the voltage close to $150V$.

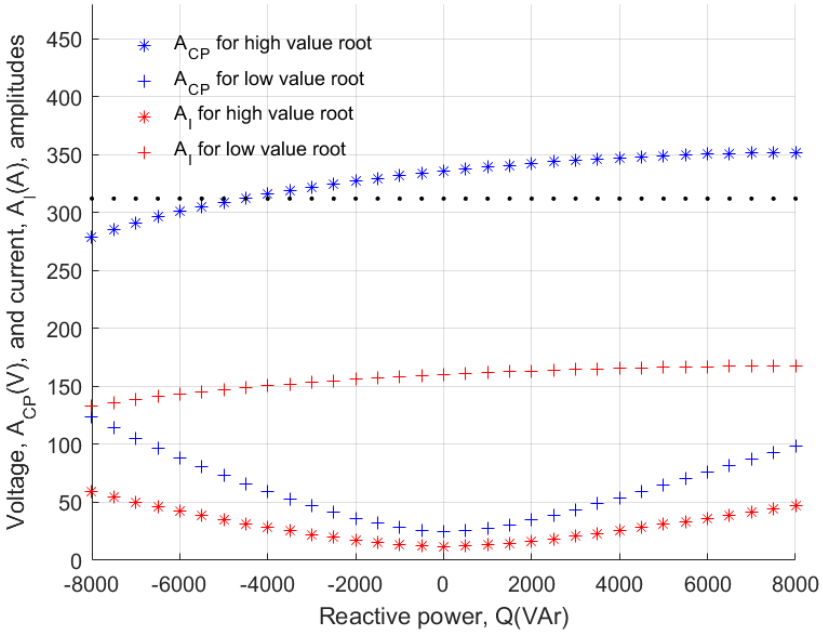

Figure 2.6: A_{CP} and A_I for $P = 2kW$ and the reactive power varies from $-8000kVAr$ to $8000kVAr$ (extract from [15]).

The Fig. 2.7 presents the behaviour of the grid phase shift when the reactive power is changed. Again, from the figure, one can realized that the solution for the high value root shows less variation with respect the other solution.

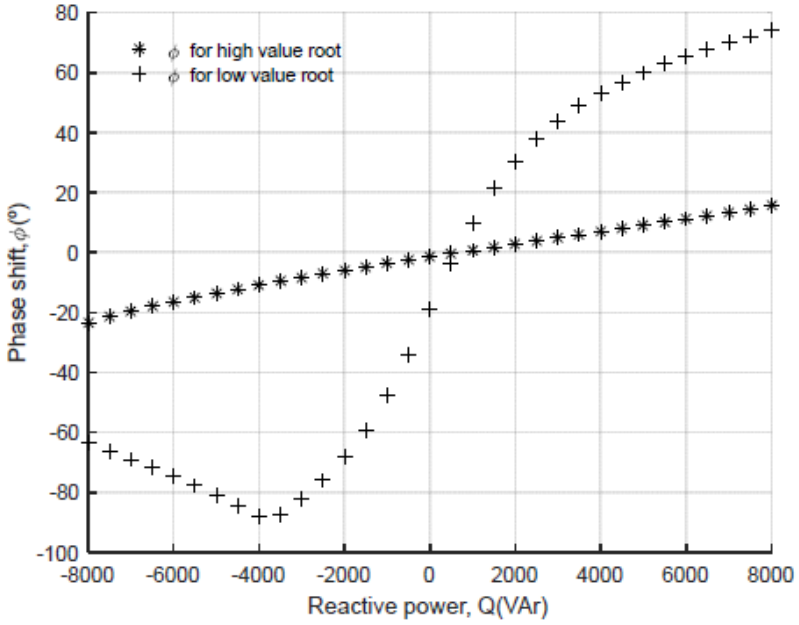

Figure 2.7: ϕ for $P = 2kW$ and the reactive power varies from -8000 to 8000 (extract from [15]).

2.4 Perfect amplitude regulation of the voltage at the connection point (Weak Grid)

Assuming that the PV inverter is properly controlled such that is delivering the desired active power, P^*, and the amplitude of the voltage at the connection point is regulated to the value (reference) of the ideal grid source, A, the equation of the network is given by:

$$A\sin(\omega t) = A_I|Z_g|\sin(\omega t - \theta + \theta_{Z_g}) + A\sin(\omega t + \phi) \tag{2.17}$$

which can be rewritten as:

$$A\sin(\omega t) - A\sin(\omega t + \phi) = A_I|Z_g|\sin(\omega t - \theta + \theta_{Z_g}) \tag{2.18}$$

Recalling the trigonometry property: $\sin\alpha - \sin\beta = 2\cos(\frac{\alpha+\beta}{2})\sin(\frac{\alpha-\beta}{2})$, the left hand side term of the equation can be expressed as:

$$A\sin(\omega t) - A\sin(\omega t + \phi) = -2A\cos(\omega t + \frac{\phi}{2})\sin(\frac{\phi}{2}) \tag{2.19}$$

or, equivalently,

$$A\sin(\omega t) - A\sin(\omega t + \phi) = 2A\sin(\omega t + \frac{\phi}{2} - \frac{\pi}{2})\sin(\frac{\phi}{2}) \tag{2.20}$$

Therefore,

$$A_I|Z_g|\sin(\omega t-\theta+\theta_{Z_g})=2A\sin(\omega t+\frac{\phi}{2}-\frac{\pi}{2})\sin(\frac{\phi}{2}) \tag{2.21}$$

which leads to the following system of equations:

$$A_I|Z_g|=2A\sin(\frac{\phi}{2})sign(\phi), \tag{2.22a}$$

$$\theta_{Z_g}-\theta=\frac{\phi}{2}-\frac{\pi}{2}sign(\phi), \tag{2.22b}$$

that, together with the expressions of the active power, $P^*=\frac{AA_I}{2}\cos\theta$, and the reactive power, $Q^*=\frac{AA_I}{2}\sin\theta$, allow to find the values of the required reactive power, Q^*, the amplitude of the injected current, A_I, the phase shift between the current and the voltage in the connection point, θ, and the phase shift between the grid source and the output voltage of the PV inverter, ϕ. Summarizing, the system equations to be solved are given by:

- $A_I|Z_g|=2A\sin(\frac{\phi}{2})sign(\phi)$
- $\theta_{Z_g}-\theta=\dfrac{\phi}{2}-\frac{\pi}{2}sign(\phi)$
- $P^*=\frac{AA_I}{2}\cos\theta$
- $Q^*=\frac{AA_I}{2}\sin\theta$

Then, replacing the second one and the third one to the first equation, one gets:

$$\frac{2P^*}{A}\frac{1}{\cos\theta}|Z_g|=2A\sin\left(\theta_{Z_g}-\theta+\frac{\pi}{2}sign(\phi)\right)sign(\phi) \tag{2.23}$$

which can be rewritten as

$$\frac{P^*}{A^2}|Z_g|=\cos\theta\sin\left(\theta_{Z_g}-\theta+\frac{\pi}{2}sign(\phi)\right)sign(\phi) \tag{2.24}$$

Recalling the trigonometry property: $\sin\alpha\cos\beta=\frac{1}{2}(\sin(\alpha+\beta)+(\sin(\alpha-\beta))$, the equation becomes:

$$\frac{P^*}{A^2}|Z_g|sign(\phi)=\frac{1}{2}\sin\left(\theta_{Z_g}+\frac{\pi}{2}sign(\phi)-2\theta\right)+\sin\left(\theta_{Z_g}+\frac{\pi}{2}sign(\phi)\right) \tag{2.25}$$

and, finally, one gets:

$$\theta = \frac{1}{2}(\theta_{Z_g} + \frac{\pi}{2} sign(\phi) - \sin^{-1}\left(\frac{P^*}{A^2}|Z_g| sign(\phi) - \sin\left(\theta_{Z_g} + \frac{\pi}{2} sign(\phi)\right)\right) \tag{2.26}$$

From this solution, the values of ϕ, A_I and Q^*, can be obtained by subsequently applying the last three equations. Notice that the above equation has two different solutions depending of the sign of the phase shift of the grid voltage.

Simulations Simulations in the following, in the Fig.2.8 and in the Fig. 2.9, show respectively the curves of voltage amplitude at connection point and trends of active and reactive output powers and the input power (from the PV array) for the real behavior of the system.

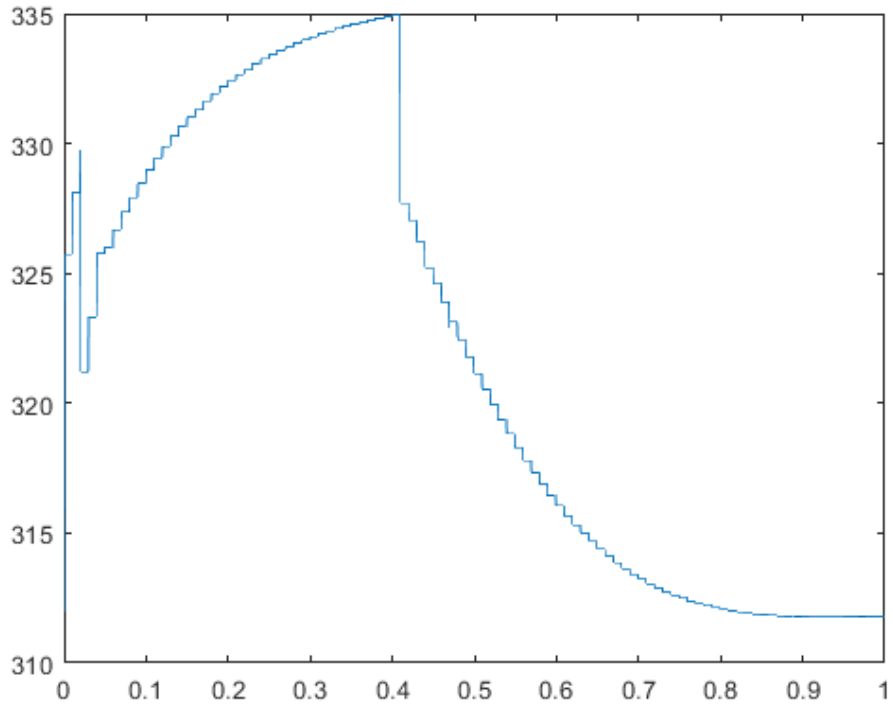

Figure 2.8: Voltage amplitude of connection point when the grid impedance is fixed at the values $R_g = 2\Omega$ and $L_g = 2mH$, active power is fixed at the value $P = 2000W$ and reactive power changes at $t = 0.4s$ from $Q = 0kVAr$ to $Q = -4.570kVAr$

In this picture is observable that during the first $0.4s$ the power control is

not enable yet and in this part is shown a free behavior and, as can be seen, the voltage amplitude is at a wrong value. At $t = 0.4s$ the power control is enable and the voltage amplitude goes to at correct values $A_{CP} = 312V$. The transient is similar to an exponential trend and the duration is $0.35s$. After the transient the voltage amplitude is stable at the nominal value. Also in this picture is observable that until $t = 0.4s$ the power control loop

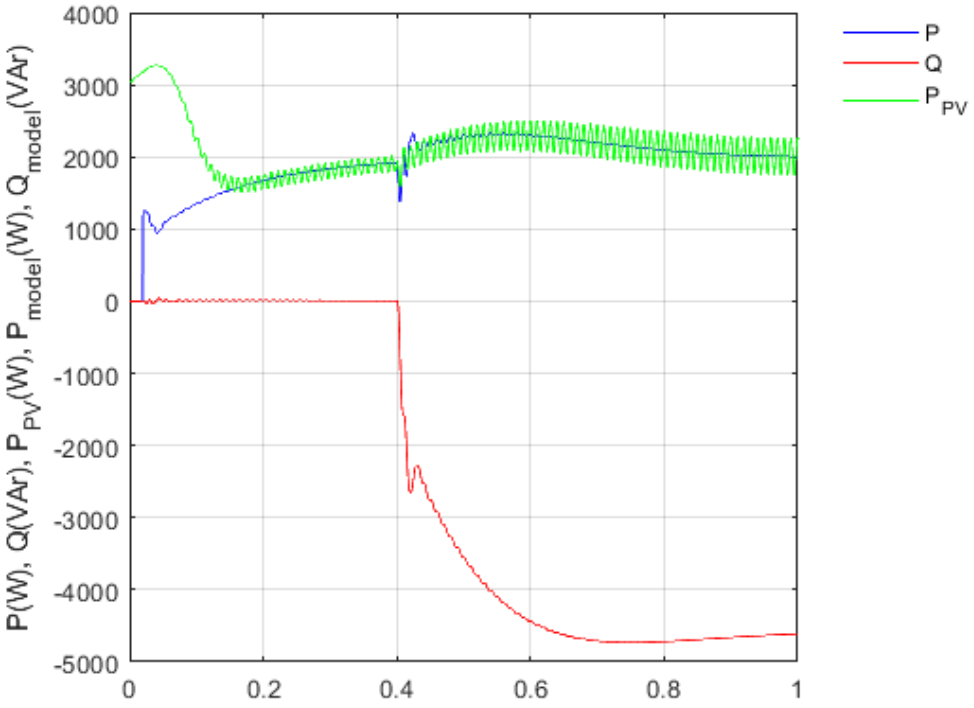

Figure 2.9: Variation of active and reactive power when the grid impedance has been fixed at the values $R_g = 2\Omega$ and $L_g = 2mH$, active power has been fixed at the value $P = 2kW$ and reactive power changes at $t = 0.4s$ from $Q = 0kVAr$ to $Q = -4.570kVAr$

is inactive. After, the power regulation begins, where starts up a transient of $0.4s$, that brings the active and reactive power values at the reference values. During the transient notice a quickly and little overshoot for the active power and another very little for reactive power corresponding.

Chapter 3

Closed-loop system modelling and stability analysis

As seen so far, when the PV inverter is connected an ideal grid, where the output impedance has only resistive part, the system needs only two control loops: one control regulator used to track the MPPT (maximum power point tracker) and used to regulate the PV array output voltage in order to guarantee that the system operates at the MPP of the PV array and another one that controls the inductor current to ensure that it is in phase with v_{CP}, that is the $PF = 1$.

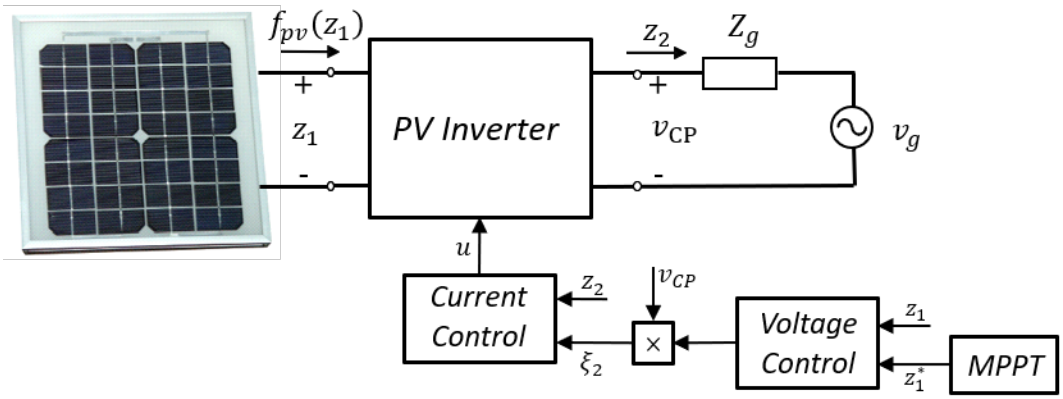

Figure 3.1: Power control for a PV inverter

When the PV inverter is connected to a weak grid the amplitude of the voltage at the connection point is sensitive and depends on the grid impedance. Changing the ratio $\frac{X}{R}$, the power factor will change, so is not more equal to the ideal case is $PF = 1$. Changing this value it has been created a variation of the amplitude A_{CP} and it has been created a phase shift between the voltage and the current. This is an important problem because the system

results instable and, in this condition, the PV inverter circuit is unusable. A good solution is to design a control loop which regulates the active and reactive power that the system supplies at the connection point in order to obtain the desired value of A_{CP}. Then, in the real case the system needs a third regulator.

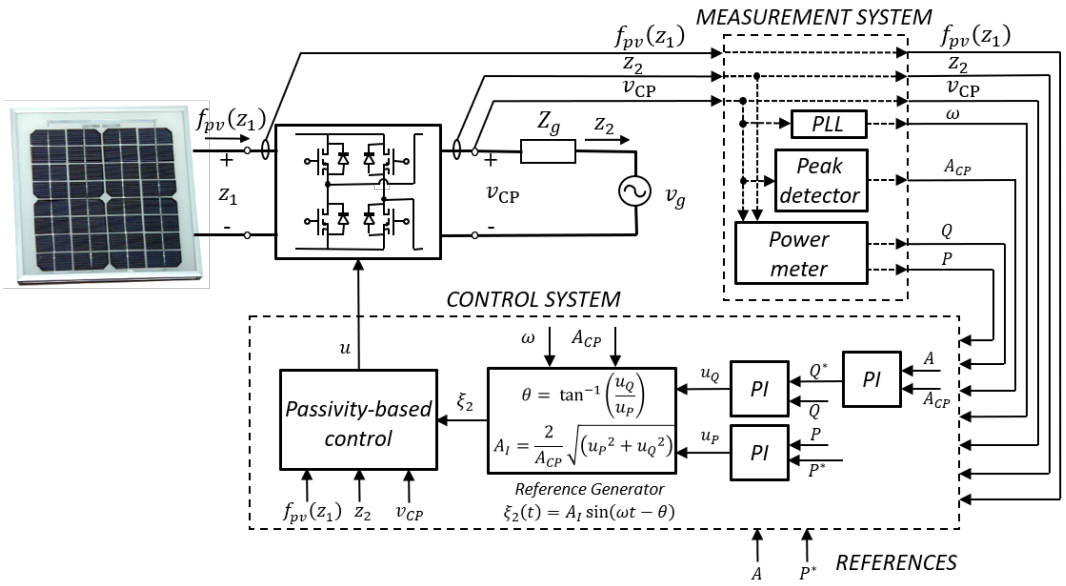

Figure 3.2: Control scheme weak grid (extract from [35]).

In the Fig.3.2 has been shown the two control loops explained in following.

- An **inner loop** to track the reference current such that the required active and reactive power are injected to the grid. (Passivity-based controller).
- A **outer loop** composed by PI controllers that ensures the regulation of P and Q toP^* and Q^* and generates the required signals to determine the current reference for the inner loop.

The control of the active and the reactive PV inverter power will help the grid (at least at the connection point of the PV system) to be in compliance with the quality standards, (i.e. amplitude setting and frequency regulation, among others).

Notice that the power regulation process is highly non-linear because:

- The PV inverter is a nonlinear system.
- The PV array presents a nonlinear characteristic which changes with the irradiance (and the temperature).
- The relationships among the amplitude and phase shift of the injected current and the active and the reactive power are highly nonlinear.
- The grid impedance could be unknown.

The non-linear caracteristic is observable from the relationship between A_{CP} and the values of P and Q has been calculated in the section 1.3 and reported shown below:

$$A_{CP} = \sqrt{\frac{A^2 + 2\Gamma\cos(\psi) + \sqrt{(A^2 + 2\Gamma\cos(\psi)^2)} - 4\Gamma^2}{2}} \tag{3.1}$$

where $\Gamma = 2|Z_g|\sqrt{P^2 + Q^2}$ and $\psi = -tan^{-1}(\frac{Q}{P}) + \theta_{Zg}$.
For this is necessary a linearization, assuming that the PV inverter operates in its steady-state:

$$\begin{gathered} v_g = A\sin(\omega t) \\ v_{CP} = A\sin(\omega t - \phi) \\ z_2(t) = A_I\sin(\omega t - \theta - \phi) \end{gathered}$$

From the reference generator is possible to define the control signals u_P and u_Q, shown below:

$$u_P = \frac{A_{CP}A_I}{2}\cos(\theta + \phi) \tag{3.2a}$$

$$u_Q = \frac{A_{CP}A_I}{2}\sin(\theta + \phi) \tag{3.2b}$$

Therefore, recalling the output power of PV inverter: $P = \frac{A_{CP}A_I}{2}\cos\theta$ and $Q = \frac{A_{CP}A_I}{2}\sin\theta$, it can be apllied the trigonometric properties, one gets:

$$P = u_P\cos\phi + u_Q\sin\phi \tag{3.3a}$$

$$Q = u_Q\cos\phi - u_P\sin\phi \tag{3.3b}$$

From these control signals, and some trigonometric operations, obtain the values of active and reactive power.
In the control scheme shown so far can be highlighted two part, the PI controllers (red) and the conditional path (green):

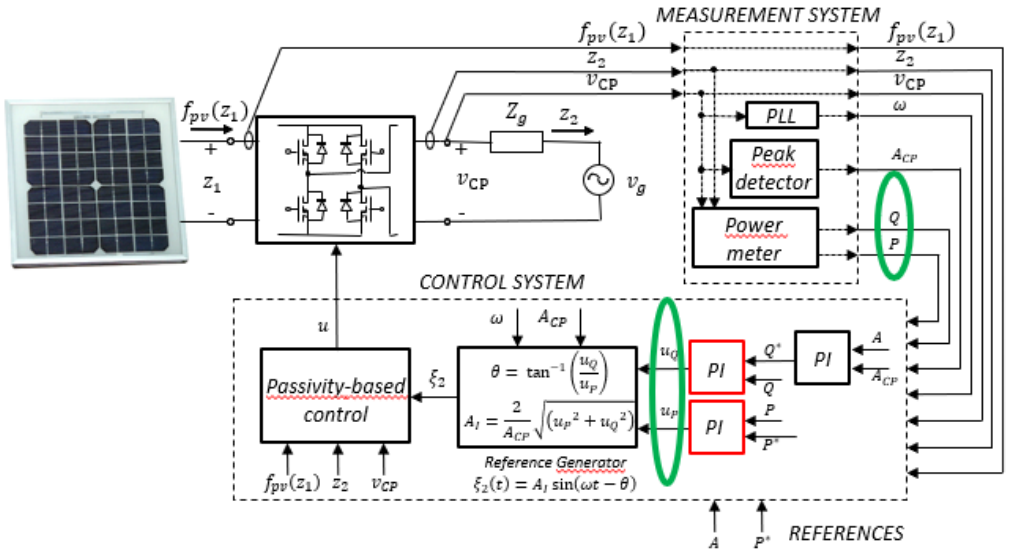

Figure 3.3: Control scheme weak grid

In order to model the closed-loop system and find rules to design the control parameters, we have to model the transfer from the power references to the amplitude at the connection point. The resultant scheme is shown in the Fig.3.4.

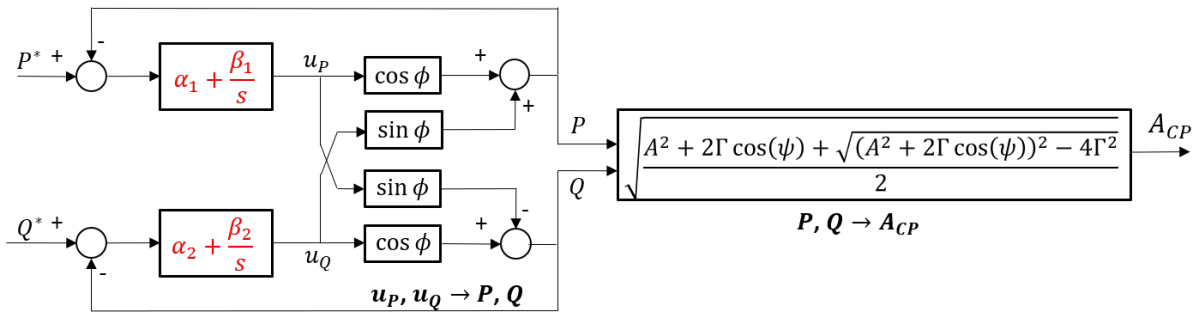

Figure 3.4: Non-linear design for the control scheme.

Note that the scheme of the PV inverter in terms of the power is given by equations 3.3.a and 3.3.b. Moreover, the PI controllers are defined with

transfer functions $G_i = G_i(s) = \alpha_i + \frac{\beta_i}{s}$. As seen previously, in order to obtain A_{CP} from the active and reactive power should be used the equation 2.1.

Recalling that A_{CP} is a non-linear function, this control scheme is not sufficient in order to obtain the value of the amplitude voltage at the connection point by the active and reactive power. For this is necessary a linearization. In a first approach, can be considered that $\cos\phi \approx \cos\phi^*$ and $\sin\phi \approx \sin\phi^*$, where ϕ^* is the reference value of the phase shift obtained when the PV inverter delivers the reference powers P^* and Q^*, i.e. at the equilibrium point. Considering the value of the phase shift ϕ, obtained when the PV inverter delivers the reference powers P^* and Q^*, it can be introduce two parameter: $\delta_1 = \left.\frac{\partial A_{CP}}{\partial P}\right|_{(*)}$ and $\delta_2 = \left.\frac{\partial A_{CP}}{\partial Q}\right|_{(*)}$.
In the Fig.3.5 is possible to note as the model changes and what is the linearization procedure used for the control scheme. So the model becomes as follows:

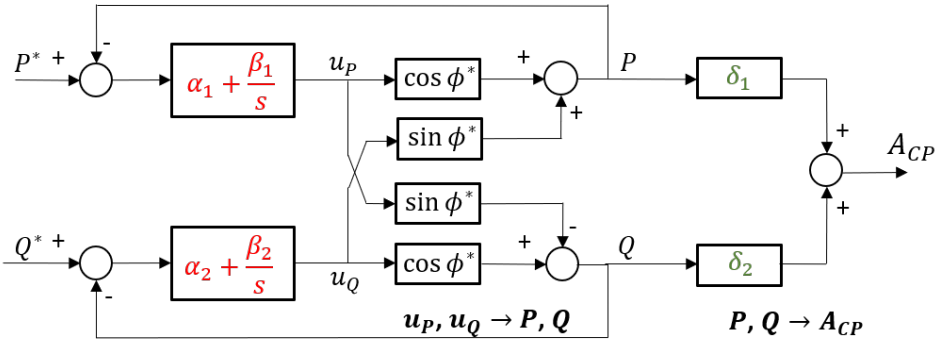

Figure 3.5: Linearization design for the control scheme.

Both the methods that will be considered use the last one model and the sensitivity parameters, but the main difference is how are obtained these parameters.

When the amplitude feedback is considered, the control system can be modelled by the scheme shown in Fig. 3.6.
In the last picture the following parameters have been defined: $\delta_1 = \left.\frac{\partial A_{CP}}{\partial P}\right|_{(*)}$ and $\delta_2 = \left.\frac{\partial A_{CP}}{\partial Q}\right|_{(*)}$.
The following analysis will determine the characteristics transfer functions of the system. First of all, it is reported the active and reactive power, which

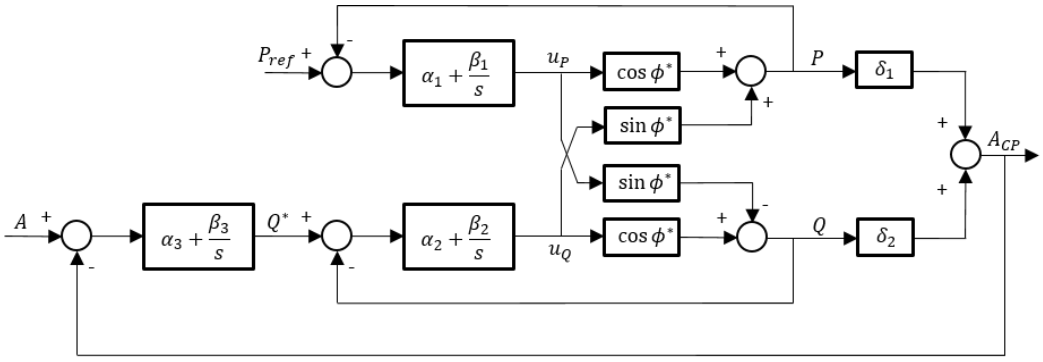

Figure 3.6: Simplified block diagram of the control scheme when the amplitude is regulated by the reactive power (extract from [35]).

can be expressed as:

$$P = u_P \cos\phi^* + u_Q \sin\phi^* = G_1 \cos\phi^*(P^* - P) + G_2 \sin\phi^*(Q^* - Q) \quad (3.4a)$$
$$Q = u_Q \cos\phi^* - u_P \sin\phi^* = G_2 \cos\phi^*(Q^* - Q) - G_1 \sin\phi^*(P^* - P) \quad (3.4b)$$

Replacing the expression of $Q^* = G_3(A - \delta_1 P - \delta_2 Q)$, the set of equations results in:

$$(1 + G_1 \cos\phi^* + \delta_1 G_2 G_3 \sin\phi^*)P = G_1 \cos\phi^* P^* + G_2 G_3 \sin\phi^* A - G_2 \sin\phi^*(1 + \delta_2 G_3)Q$$
$$(1 + G_2 \cos\phi^* + \delta_2 G_3)Q = G_2 G_3 \cos\phi^* A - G_1 \sin\phi^* P^* + (G_1 \sin\phi^* - \delta_1 G_2 G_3 \cos\phi^*)P$$

which allows to obtain the expressions of the active and reactive power as function of the active power reference and the grid amplitude:

$$P = \frac{1}{\Delta}[G_1(\cos\phi^* + G_2(1 + \delta_2 G_3))P^* + G_2 G_3 \sin\phi^* A] \quad (3.5a)$$
$$Q = \frac{1}{\Delta}[G_2 G_3(G_1 + \cos\phi^*)A - G_1(\sin\phi^* + \delta_1 G_2 G_3)P^*] \quad (3.5b)$$

where $\Delta = 1 + (G_1 + G_2)\cos\phi^* + G_2 G_3(\delta_1 \sin\phi^* + \delta_2 \cos\phi^*) + G_1 G_2(1 + \delta_2 G_3)$. Finally, as already noticed previously $A_{CP} = \delta_1 P + \delta_2 Q$, one gets:

$$A_{CP} = \frac{1}{\Delta}[G_1(\delta_1 \cos\phi^* - \delta_2 \sin\phi^* + \delta_1 G_2)P^* + G_2 G_3(\delta_1 \sin\phi^* + \delta_2 \cos\phi^* + \delta_2 G_1)A] \quad (3.6)$$

Stability can be analyzed by searching the roots of $\Delta = 0$. Replacing the transfer functions G_i in Δ, the characteristic polynomial can be written as $\Delta = \alpha_3 s^3 + \alpha_2 s^2 + \alpha_1 s + \alpha_0$, where the coefficients are:

$$\alpha_3 = 1 + \alpha_2 \alpha_3(\delta_1 \cos\phi^* + \delta_2 \sin\phi^*) + (\alpha_1 + \alpha_2)\cos\phi^* + \alpha_1 \alpha_2(1 + \delta_2 \alpha_3)$$

$$\alpha_2 = (\alpha_2\beta_3 + \alpha_2\beta_2)(\delta_1 \sin\phi^* + \delta_2 \cos\phi^*) + (\beta_1 + \beta_2)\cos\phi^* + \alpha_1\beta_2 + \alpha_2\beta_1 + \delta_2(\alpha_1\alpha_2\beta_3 + \alpha_1\beta_2\alpha_3 + \beta_1\alpha_2\alpha_3)$$

$$\alpha_1 = \beta_2\beta_3(\delta_1 \sin\phi^* + \delta_2 \cos\phi^*) + \beta_1\beta_2 + \delta_2(\alpha_1\beta_2\beta_3 + \beta_1\alpha_2\beta_3 + \beta_1\beta_2\alpha_3)$$

$$\alpha_0 = \delta_2\beta_1\beta_2\beta_3$$

Finally, local stability can be analyzed by applying the Routh Stability Criteria to Δ. Notice that the values of δ_1, δ_2 and ϕ^* depend on Z_g, therefore the parameters of the transfer functions G_i must be designed in order to ensure local stability for the overall range of possible grid impedance values.

Matlab-Simulink In this paragraph are shown the implementation on Matlab-Simulink the real control scheme and the corresponding simplified model, which will be shown in the next two chapters, where are explained the linearized methods.
Below, in the Fig. 3.7, is shown the Matlab-Simulink scheme, that represent the real behaviour of the system. In fact, in this scheme are made all the blocks in which are the real functions of the network and is built in order to obtain the real behavior.

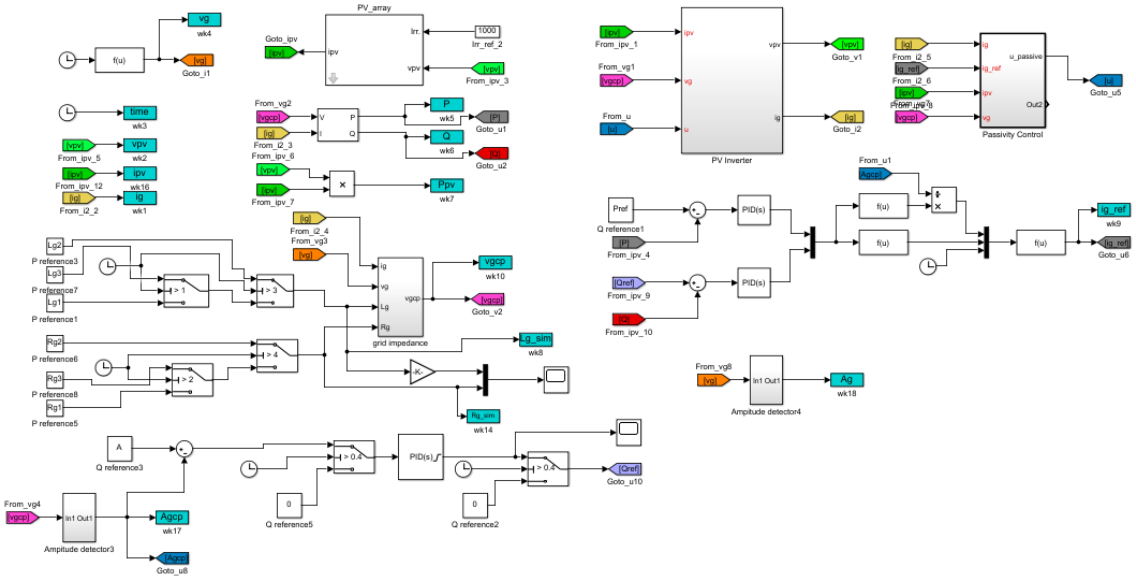

Figure 3.7: Real control scheme

In following, in the Fig. 3.11, is shown the Matlab-Simulink scheme used for

the linearized methods, as Drop method and Linearization method.
In this one, in each block, are present the part of the system seen and explained before.

- **PV array**: In this block there are as input signals a PV voltage signal and a reference value of corresponding current and in output there is the PV current signal. In following is reported the path inside the block described.

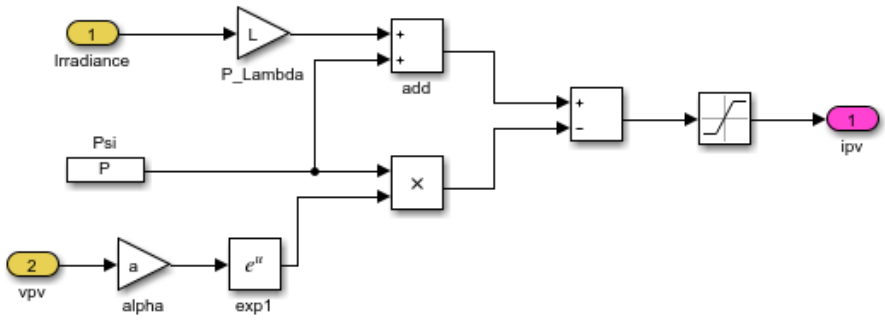

Figure 3.8: PV Array Simulink scheme

- **PV inverter**: This block is built in order to simulate an inverter and so take as input signals the control signal u for the turn on/off of the switch devices, the PV current and the voltage at connection point. As output signal, it produces the PV voltage and the grid current.

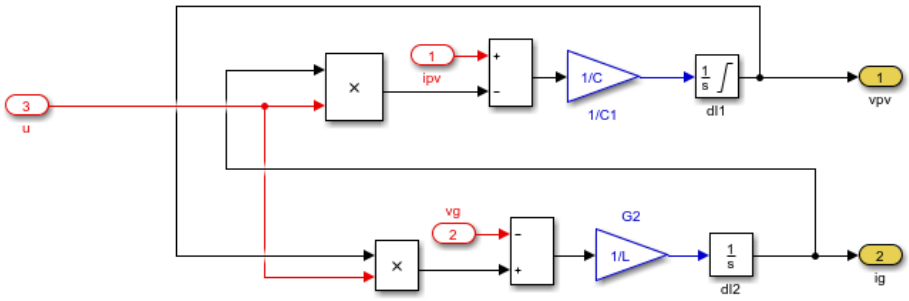

Figure 3.9: PV Inverter Simulink scheme

- **Passivity-based control**: This block implements the current control regulation seen before. It takes as input signals the reference current (inner loop), the grid current, the PV current and the voltage at connection point. As output, naturally, it produces the control signal u

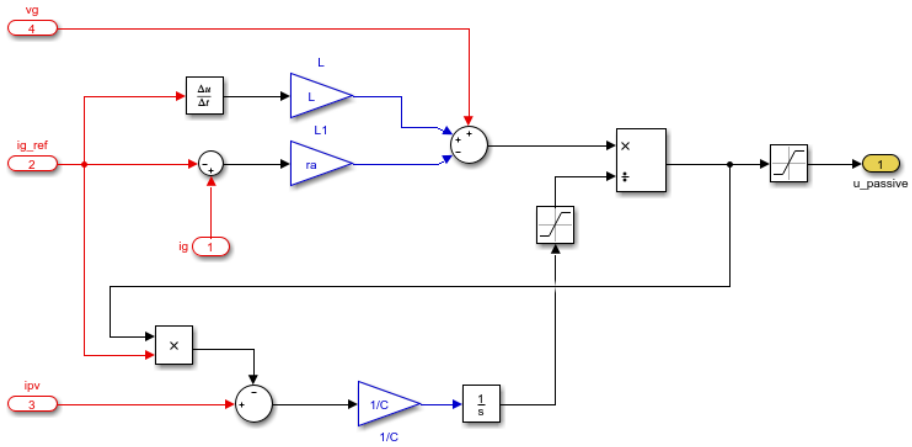

Figure 3.10: Passivity based control Simulink scheme

- **Grid impedance path**: This is a path where are as input signals the resistive and inductive part of the output impedance (are present also some paths used in order to change these values during the simulation), the grid voltage and the grid current. This block produces at the output the voltage at connection point.

- **Voltage amplitude control paths**: These are the final two paths where, regulating the output power provided at the grid, the voltage amplitude at connection point is regulated. In these paths are present three PI controllers, functions of sinus and cosinus and a control function where are used the sensitivity parameters in order to obtain the correct value of voltage amplitude at connection point.

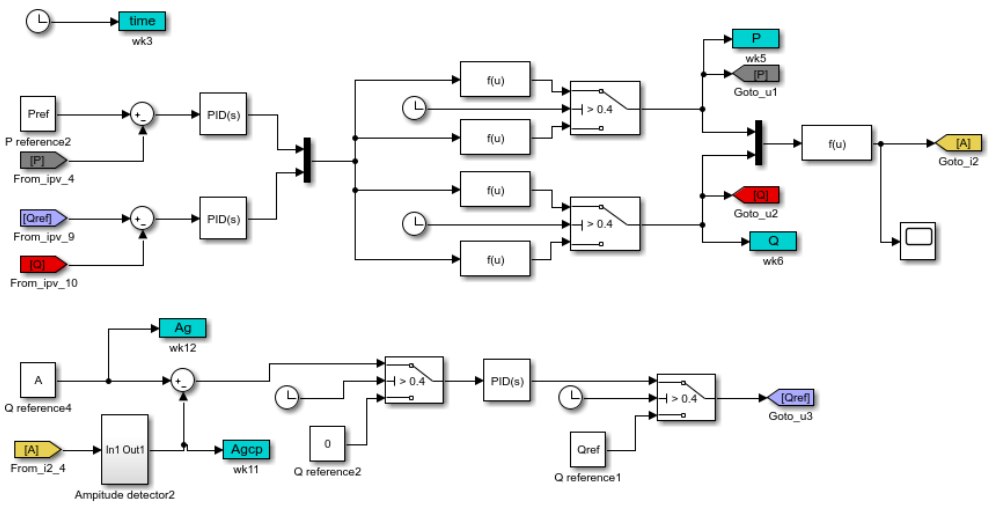

Figure 3.11: Simplified model of control scheme

In the control scheme, as explained before, there are two PI that manage the active and reactive power signals. These are used in the successive four blocks where, with the reference phase shift value, make up the combination of sine and cosine functions (see equations 2.3). From here the active and reactive power values provided at connection point have obtained and, moreover, the output signal enters in a function block where has regulated the amplitude voltage at connection point A_{CP}.
Below, there is another path that takes as input signal the A_{CP} and with a Q value has obtained the Q_{ref} value from a PI controller, used in the upper path.

Chapter 4

Modelling with drop method

In the literature there are some other methods which realize a power compensation to regulate the voltage at the connection point. One of these is the Drop method, which considers a approximation in the analytical calculus. It will be shown in following a summarized of the paper [1].

4.1 The drop method

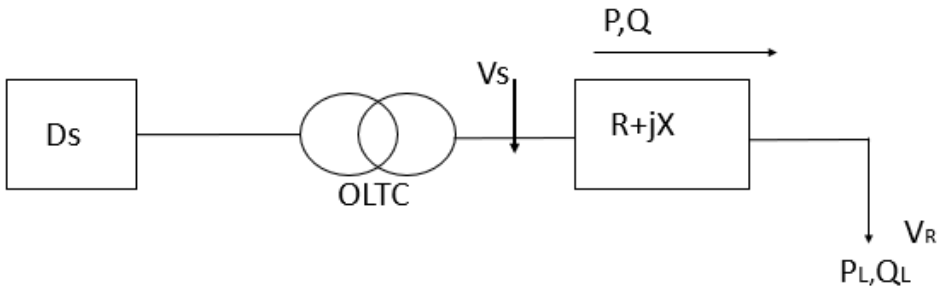

Figure 4.1: Conventional Two-bus Distribution System (extract from [1]).

The Fig.4.1 shows one scheme that can represent a passive network. Most of the distribution networks are modelled as passive networks with radial configuration and as mentioned in the literature. The flow of power, both real (P) and reactive (Q), is always from the higher to lower voltage levels. The amount of the voltage drop can be calculated from the analysis of two-bus distribution system. In the picture DS stands for the distribution system, OLTC stands for on-load tap-changer, V_S is the sending end voltage, V_R is the receiving end voltage. P and Q are the real and reactive power flowing through the distribution network to the customer, that are supplied from

distribution substation (DS) and P_L and Q_L are the real and reactive power of the load. The voltage at the sending end can be written as:

$$\hat{V_S} = \hat{V_R} + \hat{I}(R + jX) \tag{4.1}$$

Where: $(I = |\hat{I}|)$ is the phasor representation of the current flowing through the line. So, in this manner, it can write the power supplied from the distribution system:

$$P + jQ = \hat{V_S}\hat{I^*} \tag{4.2}$$

Then, the current which flows through the line is:

$$\hat{I} = \frac{P - jQ}{\hat{V_S}} \tag{4.3}$$

By this equations it can calculate the voltage:

$$\hat{V_S} = \hat{V_R} + \frac{P - jQ}{\hat{V_S}}(R + jX) = \hat{V_R} + \frac{RP - XQ}{\hat{V_S}} + j\frac{XP - RQ}{\hat{V_S}} \tag{4.4}$$

Therefore, the voltage drop between the sending end and recieving end can be written as:

$$\Delta\hat{V} = \hat{V_S} - \hat{V_R} = \frac{RP - XQ}{\hat{V_S}} + j\frac{XP - RQ}{\hat{V_S}} \tag{4.5}$$

Since the angle between the sending end voltage and the receiving end voltage is very small, the voltage drop is approximately equal to the real part of the drop and if the sending end bus is considered as reference bus, the angle of this voltage is 0, i.e., $\hat{V_S} = (|\hat{V_S}|) = V_S$. Therefore, the above equation can be approximated as:

$$\Delta\hat{V} \approx RP - XQ \tag{4.6}$$

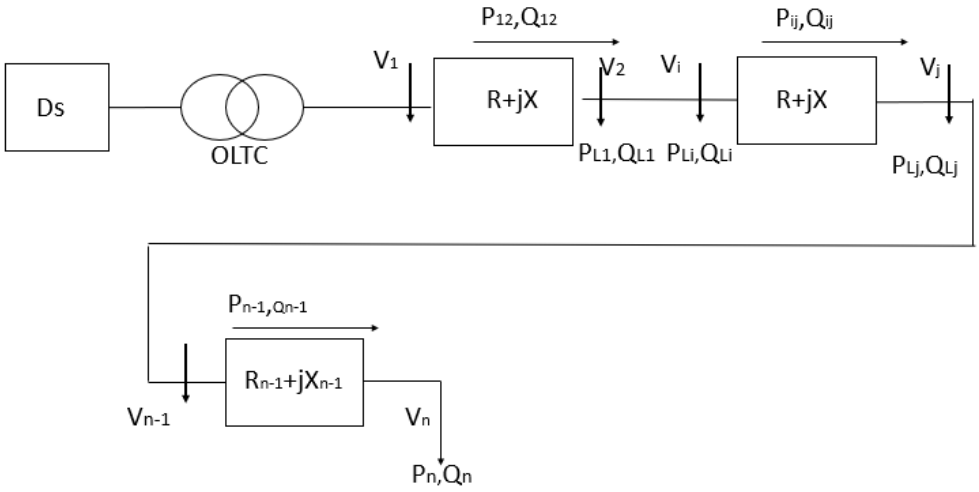

Figure 4.2: Conventional n-bus Large Distribution System (extract from [1]).

The amount of voltage variation in a large distribution network as shown Fig.4.2 can be determined by using the same formula as shown by equation (4.1). In Fig.4.2, an n-bus system is considered. The voltage drop between i^{th} and j^{th} bus can be written as:

$$\Delta \hat{V_{ij}} \approx \frac{R_{ij}P_{ij} - X_{ij}Q_{ij}}{V_{ij}} \tag{4.7}$$

Where, $\Delta \hat{V_{ij}}$ is the variation of voltage between i^{th} and j^{th} bus, R_{ij} is the resistance between i^{th} and j^{th} bus, X_{ij} is the reactance between i^{th} and j^{th} bus, V_i is the voltage at ith bus, andP_{ij} and Q_{ij} are the active and reactive power flowing from i^{th} to j^{th} bus. The voltage level at each connection point of the load is very important for the quality of the supply. Since, there are not internationally agreed rules that define the allowed steady state voltage range, the maximum voltage variation permitted on each bus is defined by some technical regulations or specific contracts.

4.2 Control scheme and equations

The control system can be modelled by the Fig.3.2 reported in the third chapter. Where have been defined the following parameters:

$$\delta_1 = \left.\frac{\partial A_{CP}}{\partial P}\right|_{(*)} = \frac{RP^*}{A_{CP}} \tag{4.8}$$

and

$$\delta_2 = \left.\frac{\partial A_{CP}}{\partial Q}\right|_{(*)} = \frac{-2\pi f L Q^*}{A_{CP}} \tag{4.9}$$

The voltage variation at the connection point is given by:

$$\Delta A_{CP} = \delta_1(P - P^*) + \delta_2(Q - Q^*) \tag{4.10}$$

in which P^* and Q^* are the active power and reactive power respectively, in the condition when $A = A_{CP}$.
Notice that is possible to evaluate the stability of system using this method watching some parameters of control design, δ_1 and δ_2 and evaluating the root locus.

Simulations Now will be studied the closed loop stability system for the Drop method looking the poles of the root locus. Below are shown the root locus plots for a specific case and will be seen all the properties of the system response for this method. In following, in the Fig. 4.3, is shown the root locus for a single case, i.e. where all the parameters of the steady state are fixed. For this simulation are fixed the output impedance ($R = 2\Omega$ and $L = 2mH$), the reference values for active and reactive power ($P^* = 2kW$ and $Q^* = -4.57kVAr$), naturally the phase shift at $\phi^* = -0.2155rad$. The couple of sensitivity parameter are: $\delta_1 = 0.0064$ and $\delta_2 = 0.002$.

It can be seen that are present three poles, two conjugated complex $s_{1,2} = -5.043 \pm j1.778$ and a real pole $s_3 = -5.709$. As expected it is a third order transfer function. From this picture it can observable that the function is stable for the of the root locus rules.

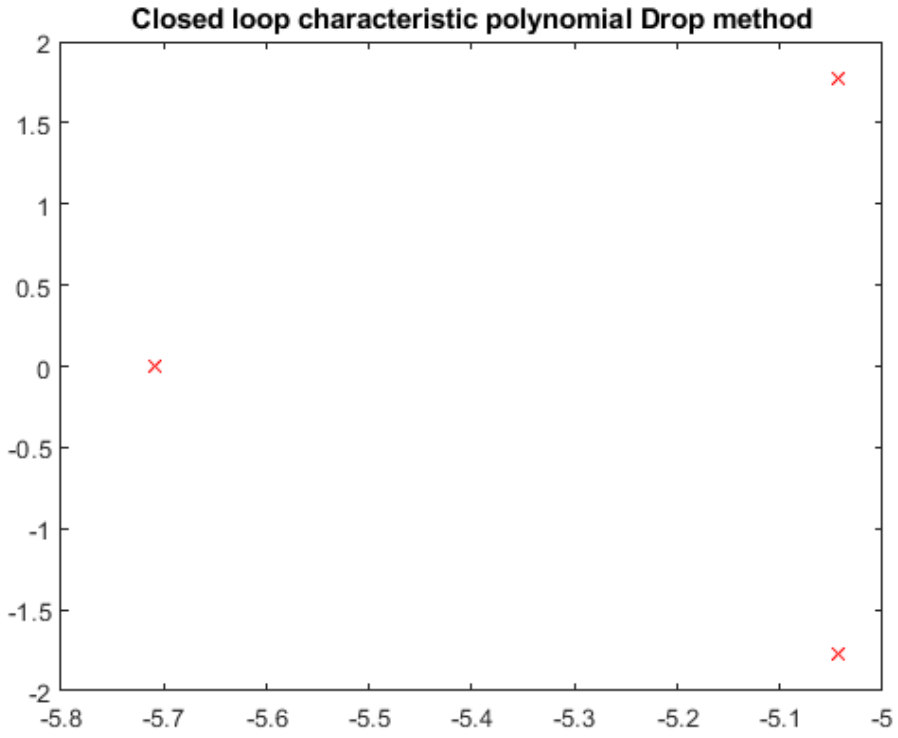

Figure 4.3: Root locus of Drop method for a single case.

Below, in Fig. 4.4, is shown the root locus when the output resistive part is fixed at $R = 2\Omega$ and reactive part changes from $1mH$ to $3mH$ by a step of $1mH$. The control parameter β_3 has been fixed at the value $\beta_3 = 2000$ and the active power changes from $500W$ to $3500W$ by a step of $500W$. Consequently, also the reactive power changes. Looking the poles on the plot is possible notice that the system response is stable.

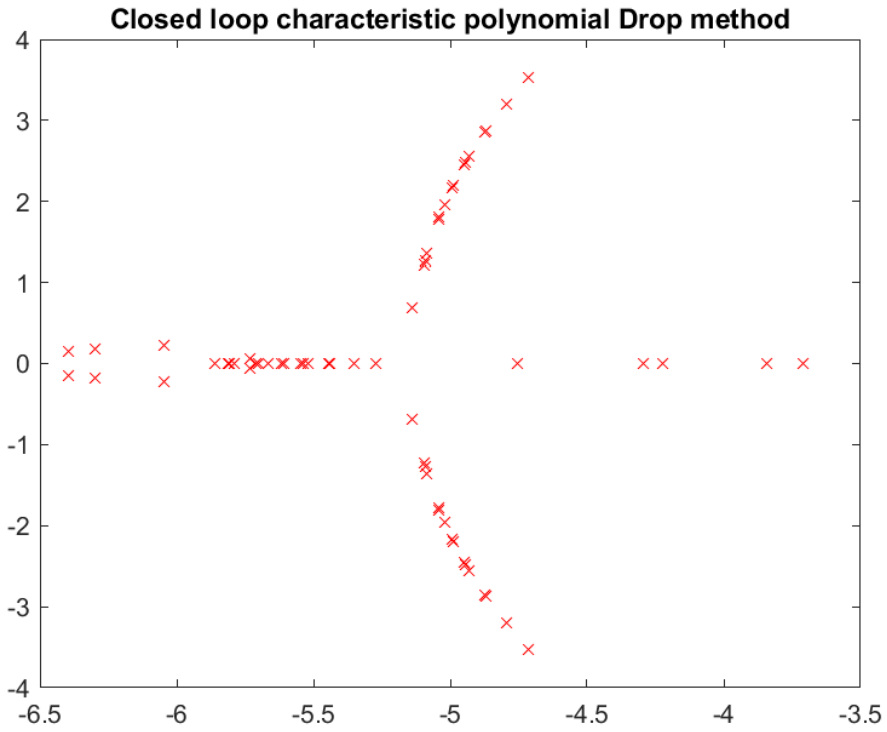

Figure 4.4: Root locus of Drop method at variation of active and reactive power fixing the value of output resistance ($R = 2\Omega$) and changing the inductance from $1mH$ to $3mH$ by a step of $1mH$.

In the Fig. 4.5 is shown the root locus with the same conditions of the previous one except for the control parameter β_3. In this case is chosen $\beta_3 = 20000$. Looking the poles on the plot is possible note that the system response is approaching to instability because is near to positive part. This condition is very important for the robustness of the system. Another difference is that the amplitude of the conjugates and complexes poles increases.

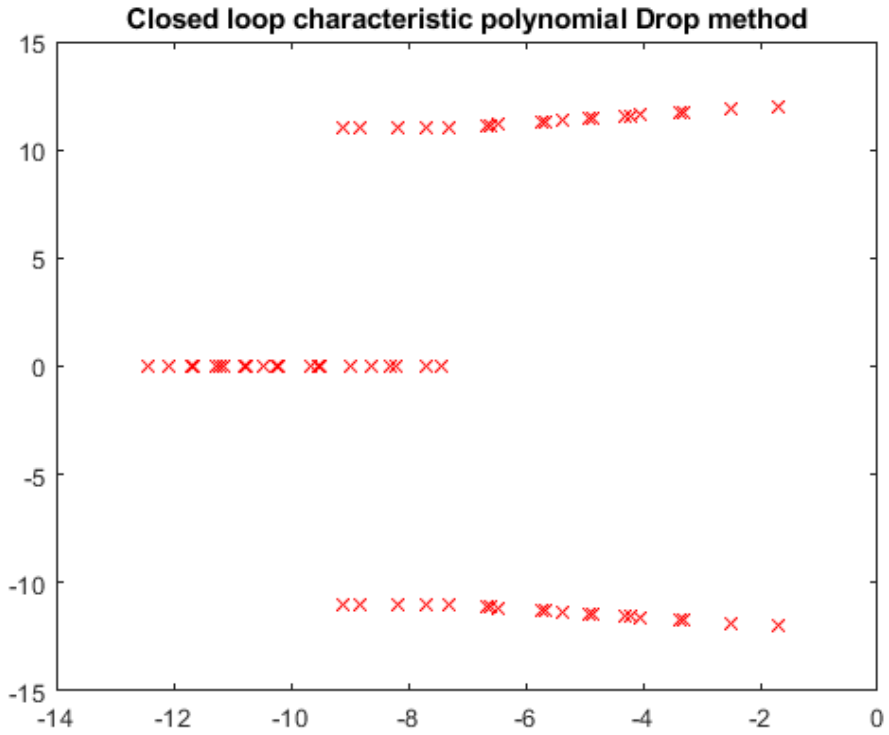

Figure 4.5: Root locus of Drop method at variation of active and reactive power when is fixed the value of output resistance ($R = 2\Omega$) and the inductance changes from $1mH$ to $3mH$ with a step of $1mH$. The other control parameters α_i and β_i are fixed.

Below will be shown the simulation plots related to Drop method, where is possible to observe the trends of main parameters of power control loop in the system in the time domain. So it is possible to study the transient and the related proprieties. These simulations are made with a Matlab-Simulink file in which is simulated the simplified model of control design scheme, where inside are present the control values related to Drop method.
The parameters used are: $R = 2\Omega$ and $L = 2mH$ (for the grid impedance), the reference active power fixed at $P^* = 2kW$, and the reactive power changes at $t = 0.4s$ from $Q = 0$ to $Q = -4.570kVAr$. The PI control parameters are: $\alpha_1 = 0.5$, $\beta_1 = 10$, $\alpha_2 = 0.5$, $\beta_2 = 10$, $\alpha_3 = 300$ and $\beta_3 = 2000$. The other parameters are: $\delta_1 = 0.0064$ and $\delta_2 = 0.002$. Naturally, also the values of reference reactive power, that in this case is fixed to $Q^* = -4.570kVAr$ and the reference phase shift $\phi^* = -0.2155rad$.
Following, will be shown the simulation plots related to Drop method, where is possible to observe the trend of main parameters of power control loop in

the system in the time domain. In the third chapter, in the Fig. 3.11, is shown the Matlab-Simulink scheme used.
This scheme represents the PV inverter connected to a non-ideal grid with an equivalent impedance of a series inductance composed of an inductive part L_g and a resistive R_g. The nominal working point is $A^*_{CP} = 312V$.
The parameters used are: $R = 2\Omega$ and $L = 2mH$ (for the grid impedance), the reference active power fixed at $P^* = 2kW$, and the reactive power changes at $t = 0.4s$ from $Q = 0$ to $Q = -4.57kVAr$. The reference phase shift is $\phi^* = -0.2155rad$. The PID control parameters are: $\alpha_1 = 0.5$, $\beta_1 = 10$, $\alpha_2 = 0.5$, $\beta_2 = 10$, $\alpha_3 = 300$ and $\beta_3 = 2000$. The sensitivity parameters are $\delta_1 = 0.0064$ and $\delta_2 = 0.002$.
In the Fig. 4.6, is shown the trends of active and reactive power and the voltage amplitude at connection point, in Fig.4.7, for the simulation in object.

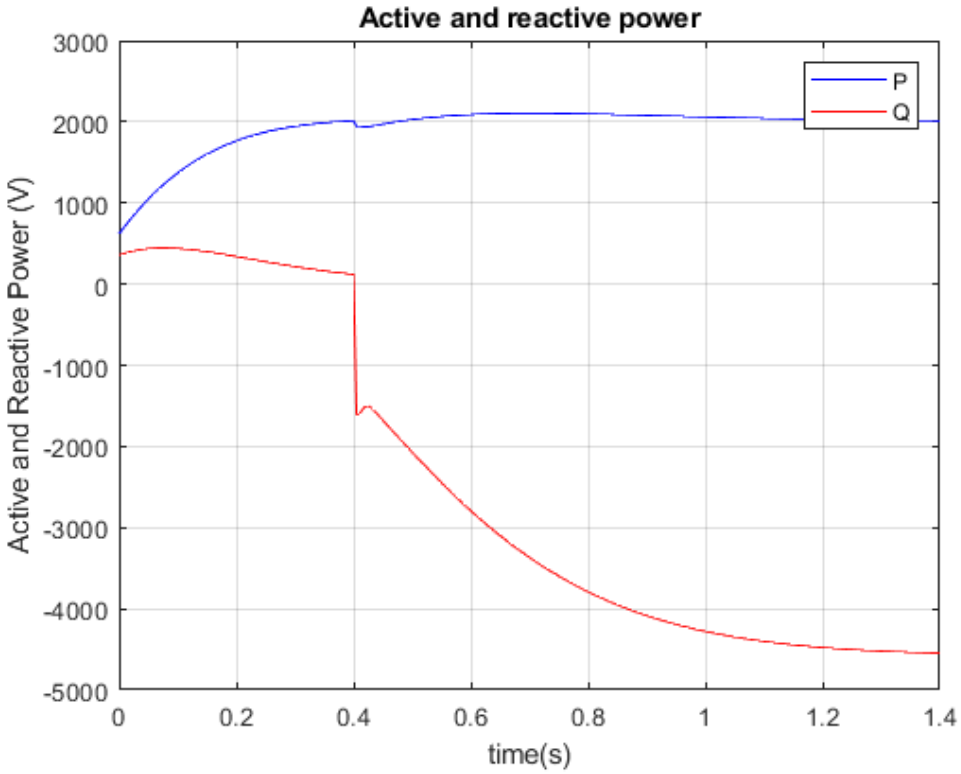

Figure 4.6: Variation of active and reactive power when the grid impedance is fixed at the values $R_g = 2\Omega$ and $L_g = 2mH$, active power is fixed at the value $P = 2kW$ and reactive power changes at $t = 0.4s$ from $Q = 0kVAr$ to $Q = -4.570kVAr$

In the Fig.4.6 notice the trend of the active and reactive power. At $t = 0.4s$

the power regulation loop is active and the values of P^* and Q^* change and after about 0.4 seconds (transient) are stabilized at the reference values. During the transient notice a little overshoot for the reactive power (about 100 kVAr), followed by a exponential decrease until the convergence at the reference value. This plot shows that the system is stable because the power trend goes to convergence at the reference values and it is happened slowly. In the Fig. 4.7 is reported the plot of voltage amplitude at connection point, when have been fixed the output impedance ($R = 2\Omega$ and $L = 2mH$), the active power at $P = 2kW$ and the reactive power changes at $t = 0.4s$ from $Q = 0$ to $Q = -4.570kVAr$. The PI control parameters are: $\alpha_1 = 0.5$, $\beta_1 = 10$, $\alpha_2 = 0.5$, $\beta_2 = 10$, $\alpha_3 = 300$ and $\beta_3 = 2000$. Moreover, the sensibility parameters are: $\delta_1 = 0.0064$ and $\delta_1 = 0.002$.

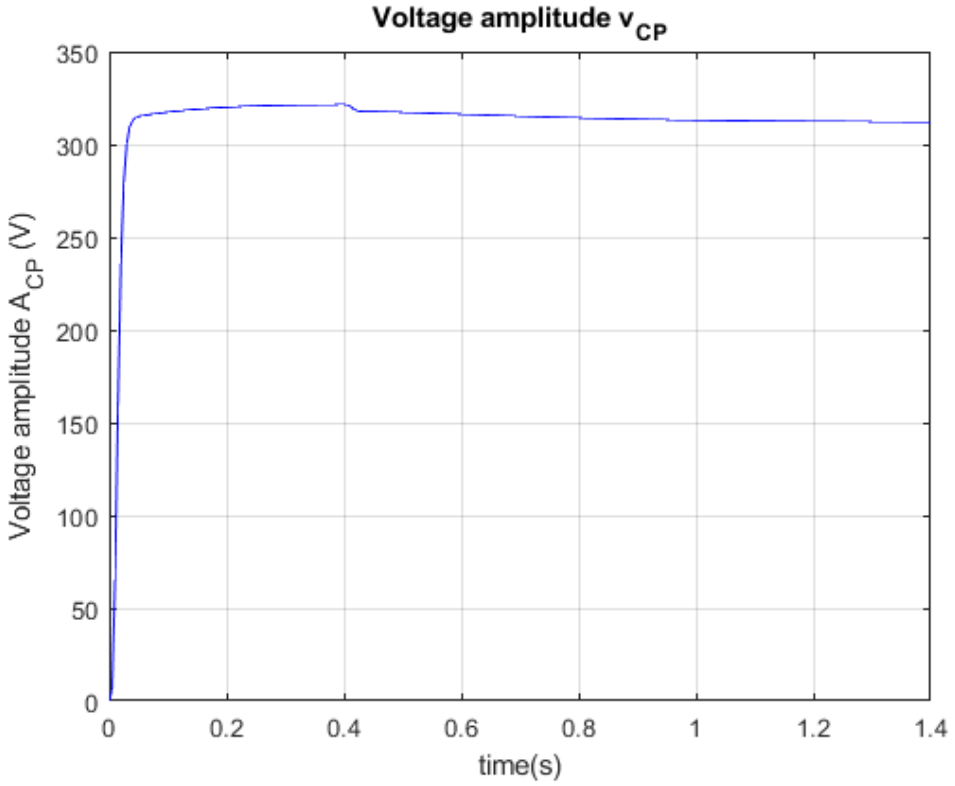

Figure 4.7: Voltage amplitude of connection point when the grid impedance is fixed at the values $R_g = 2\Omega$ and $L_g = 2mH$, active power is fixed at the value $P = 2kW$ and reactive power changes at $t = 0.4s$ from $Q = 0kVAr$ to $Q = -4.570kVAr$ in Drop method

From the last picture it can be seen that the voltage amplitude goes to the convergence without any overshoot or undershoot. This is good for the grid

because the load does not suffer voltage variation and this could be positive for the devices connected at the grid.
In order to see better the voltage trend following, in the Fig. 4.8, has been reported a zoom of the same plot.

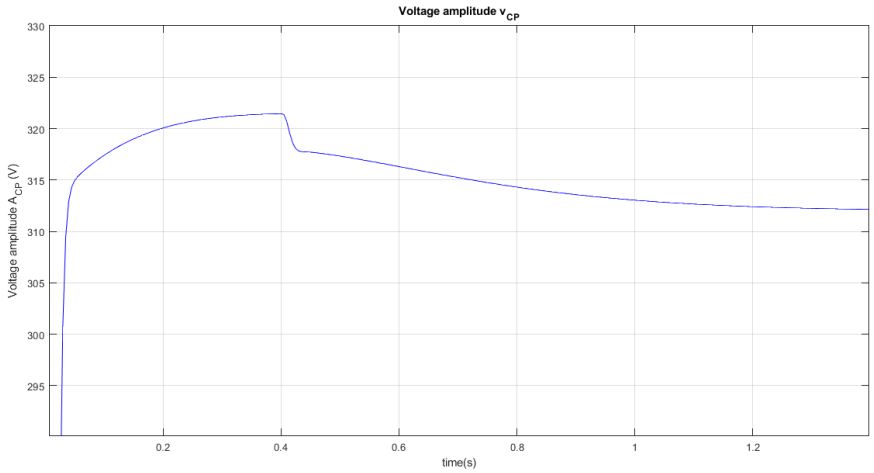

Figure 4.8: Zoom of the Fig. 4.7

Chapter 5

Modelling with linearization

Another method, more recent than the previous one, but which uses a linearization of the A_{CP} equation is the linearization method ([15], [34], [35]). The difference between the last one and this one is the different manner to obtain the sensitivity parameters and therefore also their values. In this chapter is shown the linearization method similary to have been done for the drop method.

5.1 The linearization method

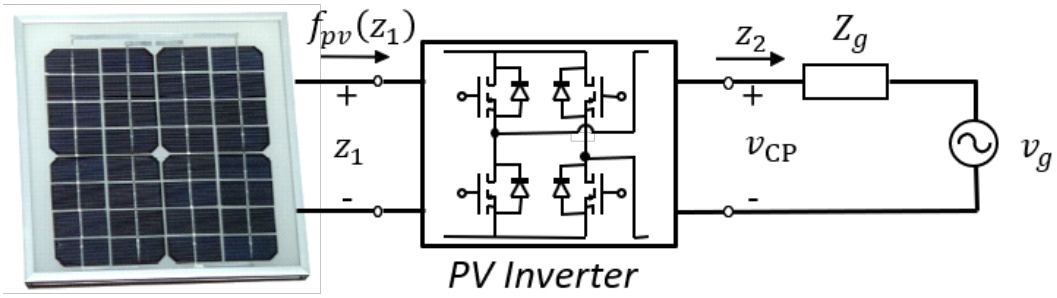

Figure 5.1: PV inverter connected to a non-ideal grid

For a PV inverter connected to a non-ideal grid, shown in Fig.5.1, the amplitude of the voltage at the connection point depends on the active and the reactive power injected to the grid. This dependence is due to the variations of the grid impedance, which consists in a series of a resistance value (R_g) and an inductance value (L_g).
This power control method regulates the amplitude of voltage at connection

point by a linearization of the real function, obtaining two control parameters, that can be defined so: $\delta_1 = \left.\frac{\partial A_{CP}}{\partial P}\right|_{(*)}$ and $\delta_2 = \left.\frac{\partial A_{CP}}{\partial Q}\right|_{(*)}$.
These control parameters, as is possible to see following, are defined in correspondence of reference values of active and reactive power, P^* and Q^* namely, and in correspondence of the reference value of phase shift ϕ^*. These three fixed values establish the equilibrium point of the system.
In following I have summarized the papers [15], [34] and [35] in order to report a short introduction which explains this method.
In correspondence of real function, the starting control scheme is shown in Fig.3.2, reported in the third chapter.
Linearizing the real function of the amplitude of voltage at connection point, also the control scheme will be linearized until to obtain the model which will be used for the following processes and simulations.

5.2 Design by linearization

Local stability of the system in object can be analyzed by a linearization the equation, that defines the voltage amplitude at the connection point as a function of the active and reactive power.
This equation is:

$$A_{CP} = \sqrt{\frac{A^2 + 2\Gamma\cos(\psi) + \sqrt{(A^2 + 2\Gamma\cos(\psi)^2)} - 4\Gamma^2}{2}} \tag{5.1}$$

where $\Gamma = 2|Z_g|\sqrt{P^2+Q^2}$ and $\psi = -tan^{-1}(\frac{Q}{P}) + \theta_{Zg}$ The linearized equation is given by:

$$A_{CP_{linear}} = A^*_{CP} + \left.\frac{\partial A_{CP}}{\partial P}\right|_{(*)}(P - P^*) + \left.\frac{\partial A_{CP}}{\partial Q}\right|_{(*)}(Q - Q^*) \tag{5.2}$$

where $(*)$ stands for the nominal working point or equilibrium point.
Defining $A_{CP} = \sqrt{\frac{f(P,Q)}{2}}$, where $f(P,Q) = f_1(P,Q) + f_2(P,Q)$, being

$$f_1(P,Q) = A^2 + 4|Z_g|\sqrt{P^2+Q^2}\cos(-\tan^{-1}(\tfrac{Q}{P}) + \theta_{Z_g})$$
$$f_2 = \sqrt{f_1(P,Q)^2 - 16(P^2+Q^2)|Z_g|^2}$$

one gets:

$$\left.\frac{\partial A_{CP}}{\partial P}\right|_{(*)} = \left(\frac{\sqrt{2}}{4\sqrt{f}}\right)\Bigg|_{(*)} \left.\frac{\partial f(P,Q)}{\partial P}\right|_{(*)} = \frac{1}{4A^*_{CP}} \left.\frac{\partial f(P,Q)}{\partial P}\right|_{(*)} = \frac{1}{4A^*_{CP}} \left(\left.\frac{\partial f1(P,Q)}{\partial P}\right|_{(*)} + \left.\frac{\partial f2(P,Q)}{\partial P}\right|_{(*)}\right) \tag{5.3}$$

and

$$\left.\frac{\partial A_{CP}}{\partial Q}\right|_{(*)} = \left(\frac{\sqrt{2}}{4\sqrt{f}}\right)\Bigg|_{(*)} \left.\frac{\partial f(P,Q)}{\partial Q}\right|_{(*)} = \frac{1}{4A^*_{CP}} \left.\frac{\partial f(P,Q)}{\partial Q}\right|_{(*)} = \frac{1}{4A^*_{CP}} \left(\left.\frac{\partial f1(P,Q)}{\partial Q}\right|_{(*)} + \left.\frac{\partial f2(P,Q)}{\partial Q}\right|_{(*)}\right) \tag{5.4}$$

Furthermore, the different partial derivatives result in:

$$\frac{\partial f_1(P,Q)}{\partial P} = \frac{4|Z_g|}{\sqrt{(P^2+Q^2)}}(P\cos\Big(-\tan^{-1}(\tfrac{Q}{P}) + \theta_{Z_g}\Big) - Q\sin\Big(-\tan^{-1}(\tfrac{Q}{P}) + \theta_{Z_g}\Big)$$
$$\frac{\partial f_1(P,Q)}{\partial Q} = \frac{4|Z_g|}{\sqrt{(P^2+Q^2)}}(Q\cos\Big(-\tan^{-1}(\tfrac{Q}{P}) + \theta_{Z_g}\Big) - P\sin\Big(-\tan^{-1}(\tfrac{Q}{P}) + \theta_{Z_g}\Big)$$

And, applying trigonometric properties yields:

$$\left.\frac{\partial f_1(P,Q)}{\partial P}\right|_{(*)} = 4|Z_g|\cos(\theta_{Z_g})$$
$$\left.\frac{\partial f_1(P,Q)}{\partial Q}\right|_{(*)} = 4|Z_g|\sin(\theta_{Z_g})$$

On the other hand,

$$\left.\frac{\partial f_2(P,Q)}{\partial P}\right|_{(*)} = \frac{1}{2f_2(P^*,Q^*)}(2f_1(P^*,Q^*)\left.\frac{\partial f_1(P,Q)}{\partial P}\right|_{(*)} - 32P^*|Z_g|^2)\left.\frac{\partial f_2(P,Q)}{\partial P}\right|_{(*)} =$$
$$\frac{4|Z_g|}{f_2(P^*,Q^*)}(f_1(P^*,Q^*)\cos(\theta_{Z_g}) - 4P^*|Z_g|)$$

$$\frac{\partial f_2(P,Q)}{\partial Q}|_{(*)} = \frac{1}{2f_2(P^*,Q^*)}(2f_1(P^*,Q^*)\frac{\partial f_1(P,Q)}{\partial Q}|_{(*)} - 32Q^*|Z_g|^2)\frac{\partial f_2(P,Q)}{\partial Q}|_{(*)} =$$
$$\frac{4|Z_g|}{f_2(P^*,Q^*)}(f_1(P^*,Q^*)\sin(\theta_{Z_g}) - 4Q^*|Z_g|)$$

Finally, the linearized equation is:

$$A_{CP_{linear}} = A^*_{CP} + \frac{1}{4A^*_{CP}}\left(\left.\frac{\partial f_1(P,Q)}{\partial P}\right|_{(*)} + \left.\frac{\partial f_2(P,Q)}{\partial P}\right|_{(*)}\right)(P-P^*) +$$
$$\frac{1}{4A^*_{CP}}\left(\left.\frac{\partial f_1(P,Q)}{\partial Q}\right|_{(*)} + \left.\frac{\partial f_2(P,Q)}{\partial Q}\right|_{(*)}\right)(Q-Q^*)$$

and, replacing the developed expressions of the partial derivatives, results in:

$$A_{CP_{linear}} = A^*_{CP} + \frac{|Z_g|}{A^*_{CP}}\cos(\theta_{Z_g})\left(1 + \frac{1}{f_2(P^*,Q^*)}\left(f_1(P^*,Q^*) - \frac{4P^*|Z_g|}{\cos(\theta_{Z_g})}\right)\right)(P - P^*) + \frac{|Z_g|}{A^*_{CP}}\sin(\theta_{Z_g})\left(1 + \frac{1}{f_2(P^*,Q^*)}\left(f_1(P^*,Q^*) - \frac{4Q^*|Z_g|}{\sin(\theta_{Z_g})}\right)\right)(Q - Q^*) \tag{5.5}$$

where

$$f_1(P^*,Q^*) = A^2 + 4\sqrt{(P^{*2} + Q^{*2})}|Z_g|\cos(-\tan^{-1}(\frac{Q^*}{P^*}) + \theta_{Z_g}) \tag{5.6}$$

and

$$f_2(P^*,Q^*) = \sqrt{f_1(P^*,Q^*)^2 - 16(P^* + Q^*)|Z_g|^2} \tag{5.7}$$

Simulations As seen in the previous chapter for the Drop method, here are shown the root locus plots for the linearization method and will be studied the closed loop stability and the properties of the system of this method.
Following is shown, in the Fig. 5.2, the root locus for a single case where all the parameters of the steady state are fixed. For this simulation are fixed the output impedance ($R = 2\Omega$ and $L = 2mH$), the reference values for active and reactive power ($P^* = 2kW$ and $Q^* = -4.57kVAr$) and, naturally the phase shift at $\phi^* = -0.2155rad$. Moreover, the sensibility parameters used are: $\delta_1 = 0.0151$ and $\delta_1 = 0.0073$.
It can be seen that are present three poles, two complex conjugate $s_{1,2} = -7.326 \pm j3.786$ and a real pole $s_3 = -6.39$. As expected, it is a third order transfer function. From this picture it can observable that the function is stable for the root locus rules.

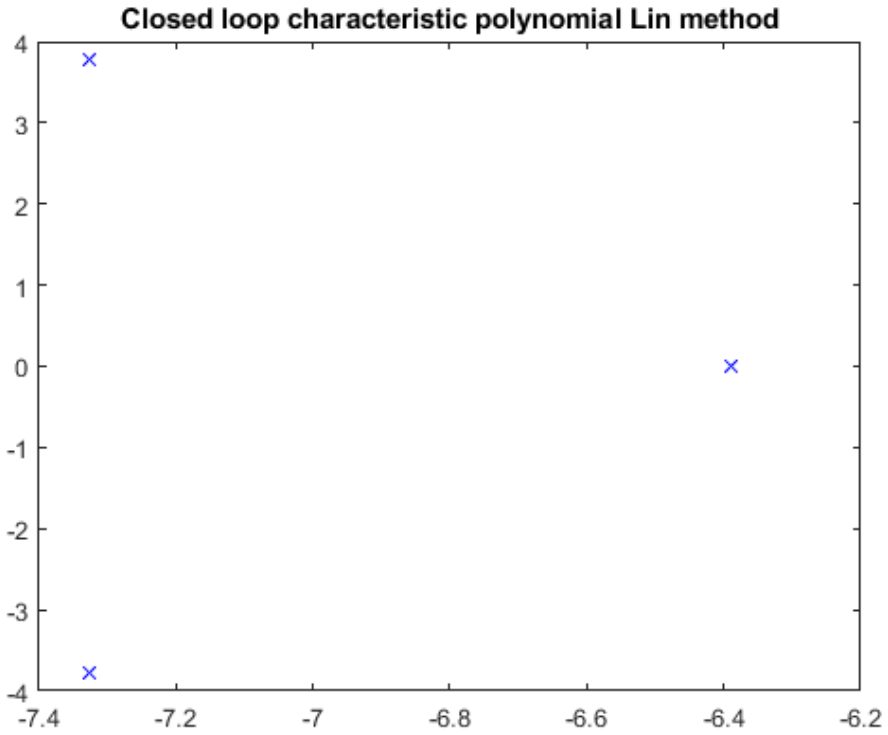

Figure 5.2: Root locus of linearization method for a single case

Below is shown in Fig. 5.3 the root locus when the output resistive part is fixed at $R = 2\Omega$ and reactive part changes from $1mH$ to $3mH$ by a step of $1mH$. The control parameter β_3 has been fixed to the value $\beta_3 = 2000$ and the active power changes from $500W$ to $3500W$ by a step of $500W$, consequently also the reactive power changes.

Looking the poles on the plot in the last picture is possible to note that the system response is stable.

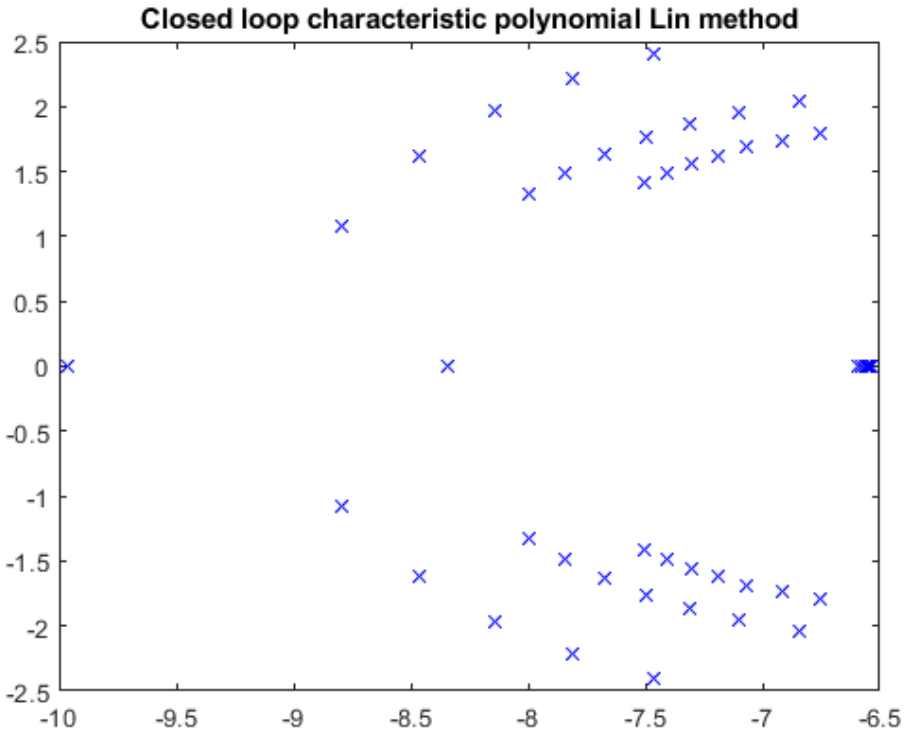

Figure 5.3: Root locus of Linearization method at variation of active and reactive power when is fixed the value of output impedance ($R = 2\Omega$) and the inductance changes from $1mH$ to $3mH$ with a step of $1mH$.$\beta_3 = 2000$.

In the Fig. 5.4 is shown the root locus with the same conditions of the previous one except for the control parameter β_3. In this case is chosen $\beta_3 = 20000$. Looking the poles on the plot is possible note that the system response continues to be stable and keeps a good robustness being far of the positive part. Another difference is that the amplitude of the conjugates complexes poles increases.

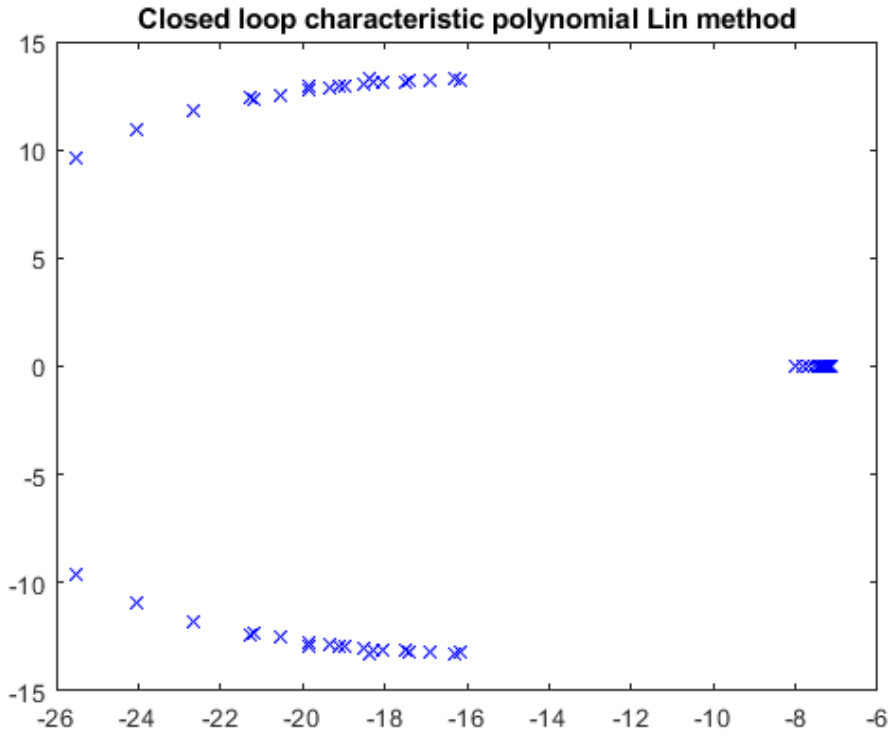

Figure 5.4: Root locus of Linearization method at variation of active and reactive power when is fixed the value of output impedance ($R = 2\Omega$) and the inductance changes from $1mH$ to $3mH$ with a step of $1mH$. $\beta_3 = 20000$.

Below will be shown the simulation plots related to Linearization method, equivalently as seen as before for the Drop method, in order to observe the trend of main parameters of power control loop in the system in the time domain. So it is possible to study the transient and the related proprieties. These simulations are made by a Matlab-Simulink file in which the simplified control design scheme has been simulated.
Following, in the Fig. 5.5, is shown the Matlab-Simulink model scheme used.

This scheme represents the PV inverter connected to a non-ideal grid with an equivalent impedance of a series inductance composed of an inductive part L_g and a resistive R_g. The nominal working point is $A^*_{CP} = 312V$. The control scheme and the equilibrium point assumed are the same that have been used previously for Drop method analysis. In this one change only some control values as $\delta_1 = 0.0151$ and $\delta_2 = 0.0073$, i.e. the sensitivity parameters.
Have been used: $R = 2\Omega$ and $L = 2mH$ (for the grid impedance), the reference active power fixed at $P^* = 2kW$, and the reactive power changes

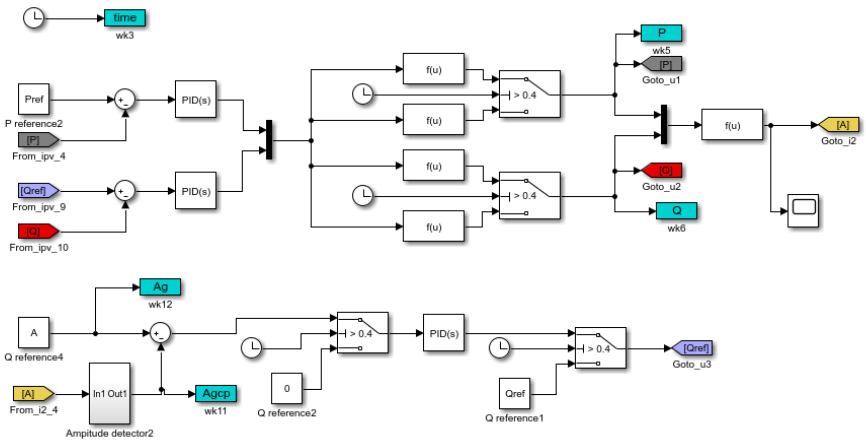

Figure 5.5: Simplified control scheme

at $t = 0.4s$ from $Q = 0$ to $Q = -4.570kVAr$.
In following, in the Fig. 5.6, has been shown the trends of active and reactive power, while the voltage amplitude at connection point has been shown in Fig.5.7.

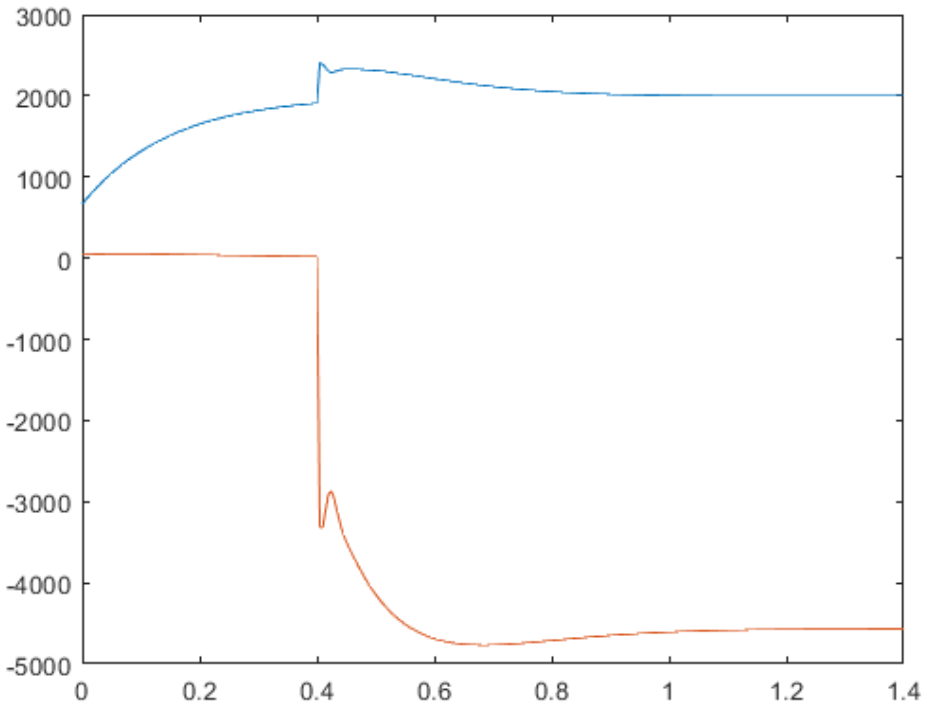

Figure 5.6: Variation of active and reactive power when the grid impedance is fixed at the values $R_g = 2\Omega$ and $L_g = 2mH$, active power is fixed at the value $P = 2kW$ and reactive power changes at $t = 0.4s$ from $Q = 0kVAr$ to $Q = -4.570kVAr$

In the Fig.5.6 notice the trends of the active and reactive power. At $t = 0.4s$, the power regulation loop is active and the values of P^* and Q^* change and in 0.3 seconds (transient) are stabilized at the reference values. During the transient notice an high overshoot for the active power of about 250 W and a corresponding overshoot for the reactive power. This picture shows that the system is stable because the powers trend go to convergence at the reference values and it is happen very fastly.

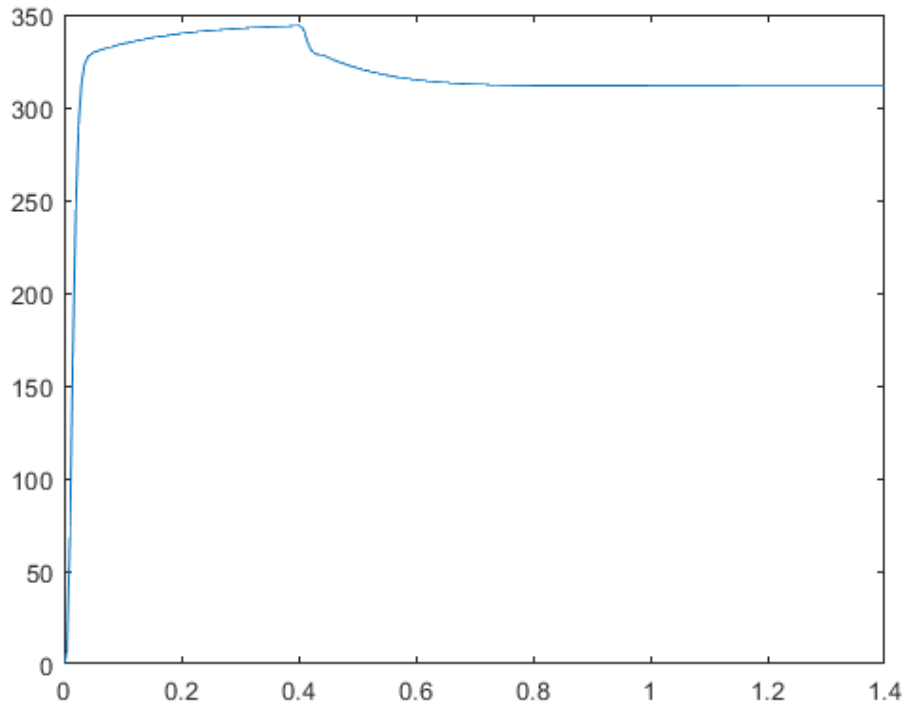

Figure 5.7: Voltage amplitude of connection point when the grid impedance is fixed at the values $R_g = 2\Omega$ and $L_g = 2mH$, active power is fixed at the value $P = 2000W$ and reactive power changes at $t = 0.4s$ from $Q = 0kVAr$ to $Q = -4.57kVAr$ in Linearization method

In the Fig.5.7 has been shown the trend of the voltage amplitude at the connection point corresponding. Initially, before that the control works, the value of the amplitude is at wrong value. At $t = 0.4s$, when the power control is activeted, the voltage goes to the nominal value fastly. As for the powers trends as here it is possible to see that the system response is stable and the voltage go to convergence.

Chapter 6

Comparison of the methods

Through the cases analyzed in the last two chapter is possible to study and analyze the approximated methods shown before. Obviously, the method which has a trend closer to the real behavior is better than the other one because is the most realistic. As seen before, both are stable and the curves of active and reactive powers and the curve of voltage amplitude converge at the referance values.
Following, in the Fig. 6.1, is shown the variation reference values of active and reactive power of the linearization behavior compared to the drop method behavior, when the PV inverter supplies an active power from $500W$ to $3500W$ and a reactive power from $-12000kVAr$ to $0kVAr$ to a grid with an equivalent impedance of a series inductance ($L_g = 2mH$) and a resistance of ($R_g = 2\Omega$). The powers change in steps of $500W$ for the active and $500kVAr$ for the reactive.

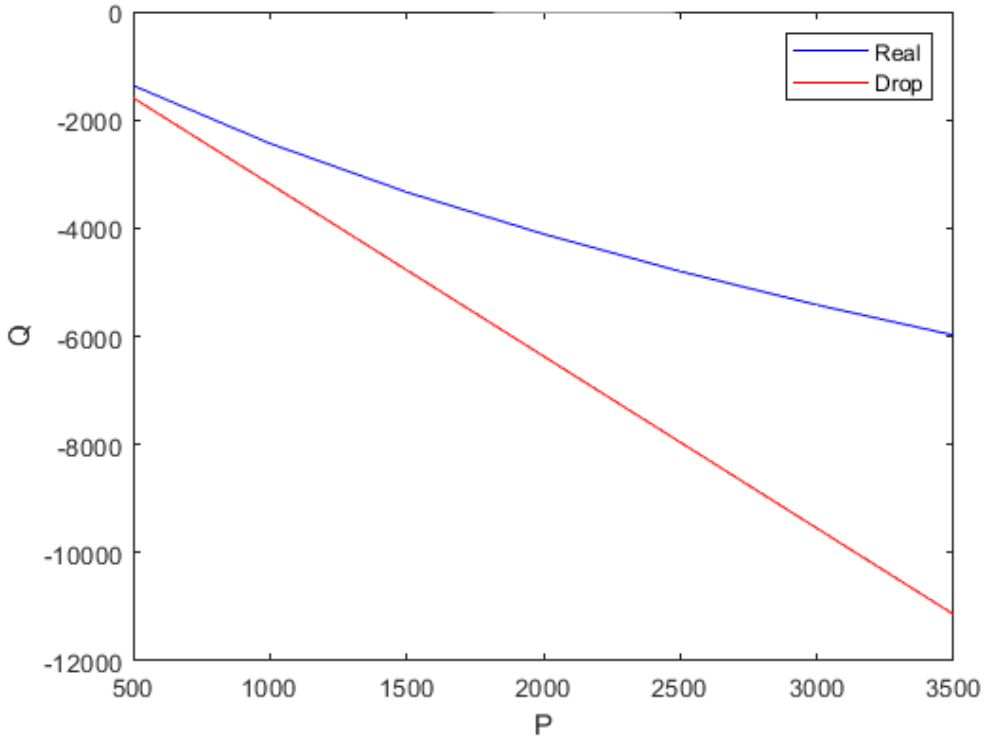

Figure 6.1: P^* and Q^* when active power varies from $500W$ to $3500W$ and the reactive power varies from $-12000kVAr$ to $0kVAr$

Note that for the low power values the trends are similar and the difference is small and therefore neglected, but increasing the active and reactive power values the difference increas, becouse the linearization behavior has an exponential trend while the drop method behavior has a linear trend.

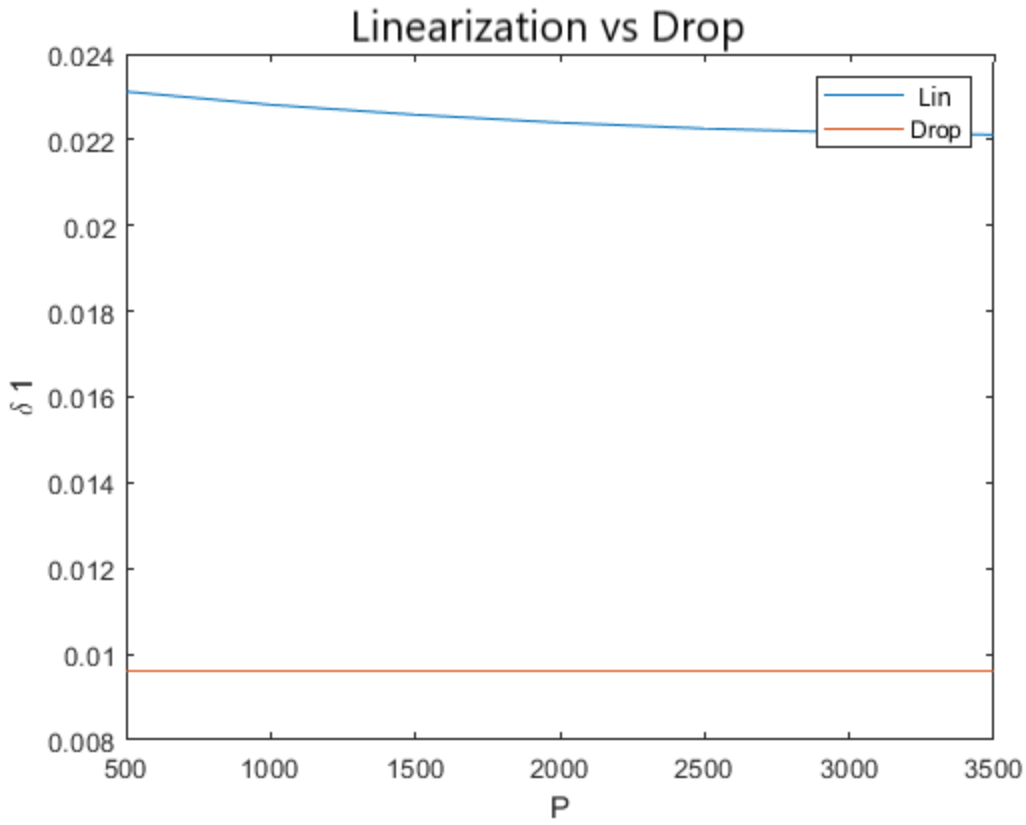

Figure 6.2: δ_1 when active power varies from $500W$ to $3500W$

The Fig. 6.2 shows the comparison of the δ_1 parameter between the linearization behavior and the drop method changing the active power value from $500W$ to $3500W$. Notice that in the drop method δ_1 is costant changing P. This because $\delta_1 = \frac{R}{A}$ in the drop method. In the linearization notice that δ_1 depends on P by a non-linear function. The difference between these two characteristics of δ_1 changes the behaviur of the control system.

The Fig. 6.3 shows the comparison of the δ_2 parameter between the real behavior and the drop method changing the active power value from $500W$ to $3500W$. Also for δ_2, notice that in the drop method behavior δ_1 is costant with the changing of P, because $\delta_2 = \frac{X}{A}$ in the drop method. In the real behavior notice that δ_1 depends on P increasing costantly when P increases. As for δ_1 as for δ_2, being a control parameters, the difference of the charatteristics changes the behavior of the control system.

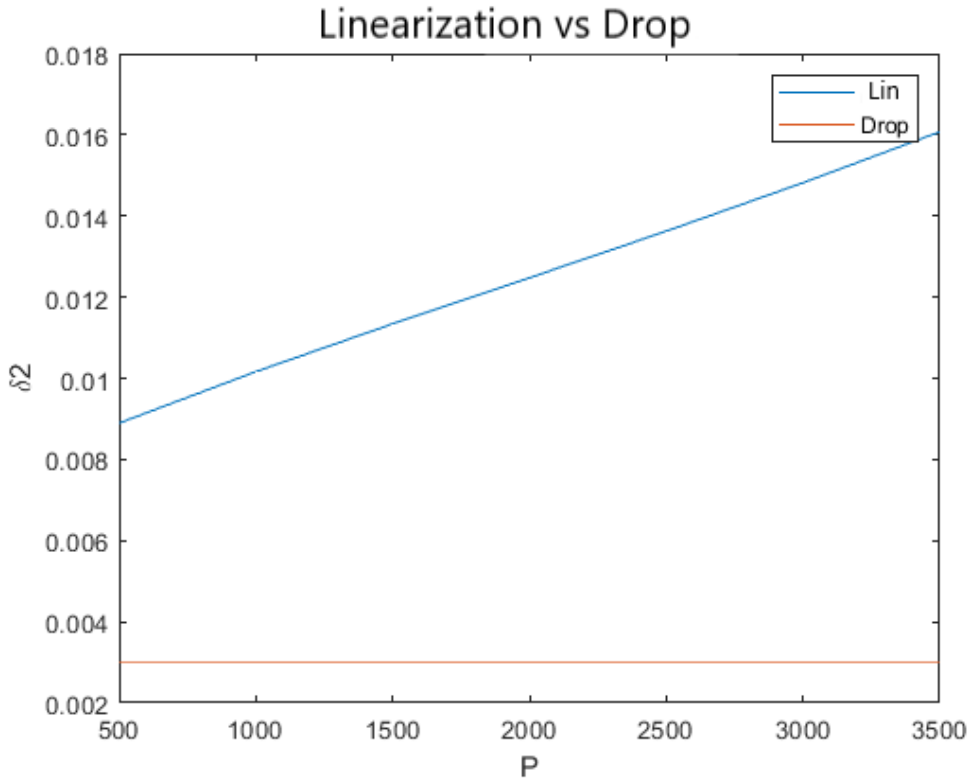

Figure 6.3: δ_2 when active power varies from $500W$ to $3500W$

Initially will be studied the case where the output grid impedance has been fixed ($R = 2\Omega$ and $L = 2mH$), the referance active power fixed at $P^* = 2kW$, the reactive power changes at $t = 0.4s$ from $Q = 0$ to $Q = -4.570kVAr$ and the phase shift has been fixed to $\phi^* = -0.2155rad$. The PI control parameters are: $\alpha_1 = 0.5$, $\beta_1 = 10$, $\alpha_2 = 0.5$, $\beta_2 = 10$, $\alpha_3 = 300$ and $\beta_3 = 2000$. While the sensitivity parameters are: $\delta_1 = 0.0064$ and $\delta_2 = 0.002$, for Drop method, and $\delta_1 = 0.0151$ and $\delta_2 = 0.0073$, for Linearization method.
For these simulations has been used the model control scheme in the Fig.3.11.

In following, this study will be deal with the Matlab-Simulink simulations seen before overlapping the results. Below, in Fig.6.4, is shown the voltage amplitude at connection point that has been compared among the real behavior, the Drop method behavior and the Linearization method behavior, where the real one is taken, naturally, as the reference.

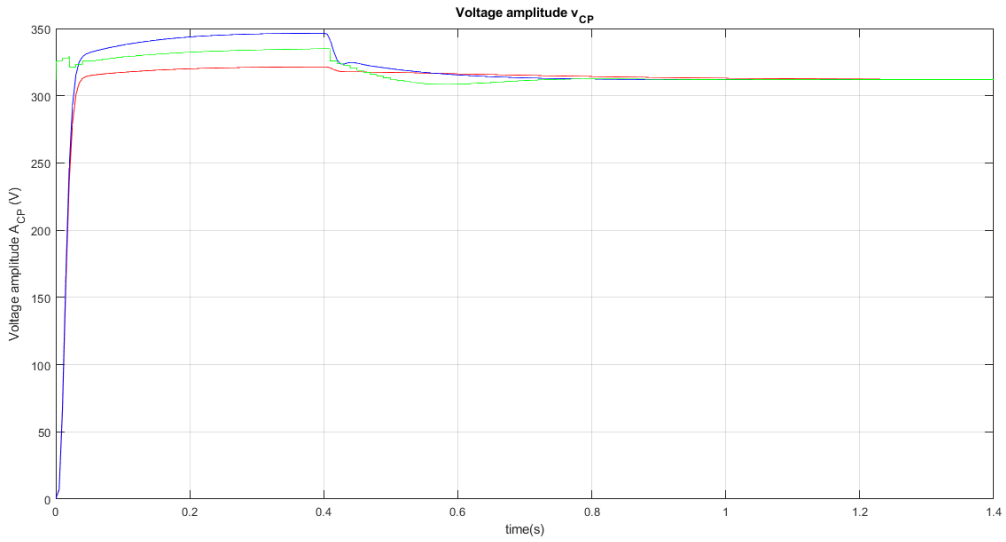

Figure 6.4: Voltage amplitude comparison

In order to see better the voltage trend following, in the Fig. 6.5, has been reported a zoom of the same plot.

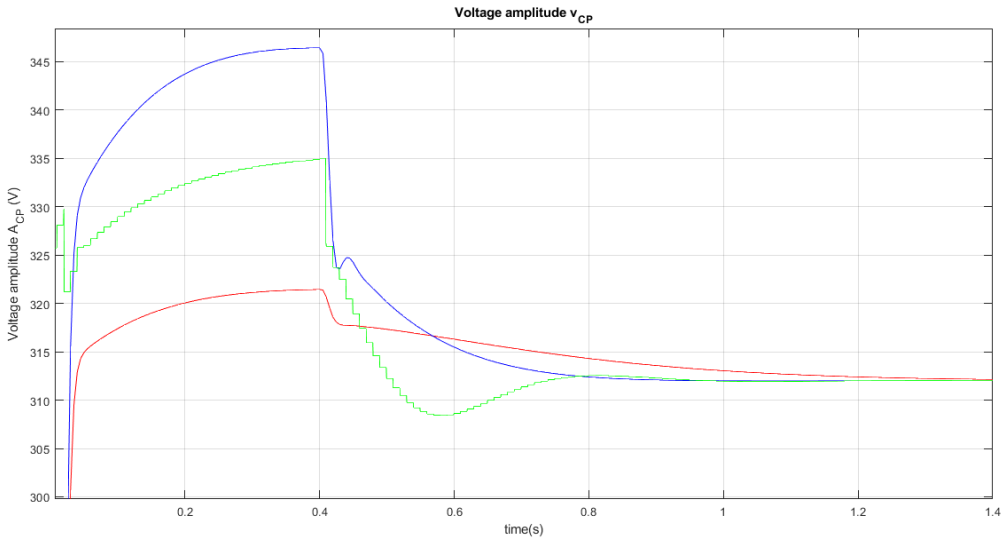

Figure 6.5: Zoom of the Fig.6.5

It can be seen that the Linearization method goes closer to the real behavior than the Drop, specially during the transient, from $t = 0.4s$, or rather when the power control loop in the system is activated. This difference is little but very important, because this means that the Linearization method has an higher accuracy.

Below, in Fig.6.6, are shown the active and reactive powers provided to the output. In the picture, infact, it has been compared among the real behavior, the Drop method and the Linearization method, where the real one is the reference.

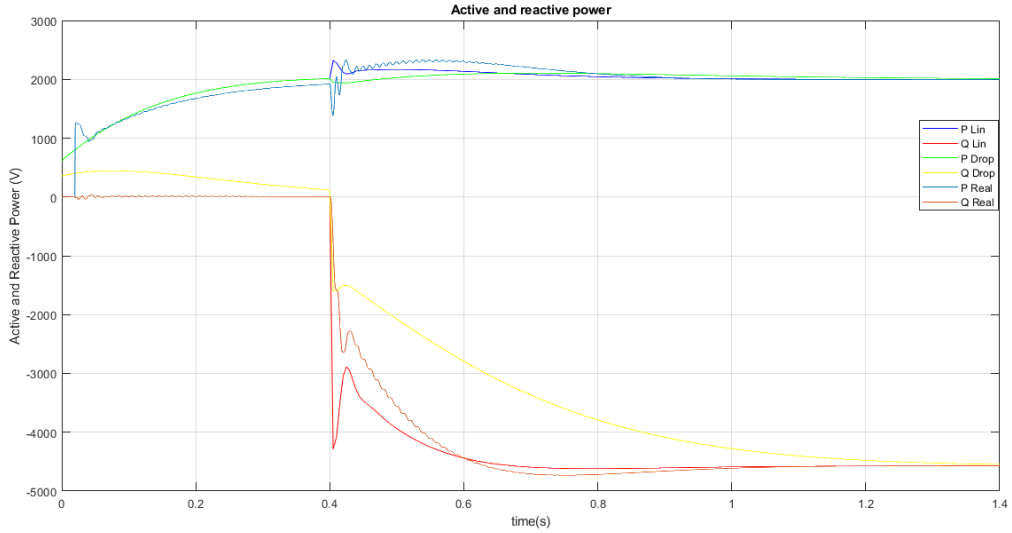

Figure 6.6: Active and reactive power comparison

In this figure is more evident the difference, specially in the reactive power. Take focus initially on the active power curves. The Drop method curve is almost linear and is without an evident overshoot, while for the real trend and the Linearization method curve, when the control loop starts up, there is a little overshoot. Also during the transient the Linearization curve is closer to real than Drop curve.
Now compare the reactive power curves. Notice easily that the Drop curve has a slower slope and seems an exponential trend, while the frame of the Linearization one is closer to real one and so it is observable an overshoot, present when the regulation starts up. Then, also during the transient, notice that the real behavior does not go immediately to the reference value, but there is a slow and little undershoot. After $0.5s$ goes to convergence value. It is explicit that the linearization curve follows better than the other one the real behavior also during the transient.

Now, changing a control parameter as β_3 from a beginning value of $\beta_3 = 1000$ to a final value of $\beta_3 = 10000$ with a step of 1000, it is possible compare again the methods. The firsts two pictures represent the real behavior and so are the references for the comparison. In the Fig.6.7 has been reported the voltage amplitude at connection point curve, while in the Fig.6.8 has been shown the active and reactive power curves.

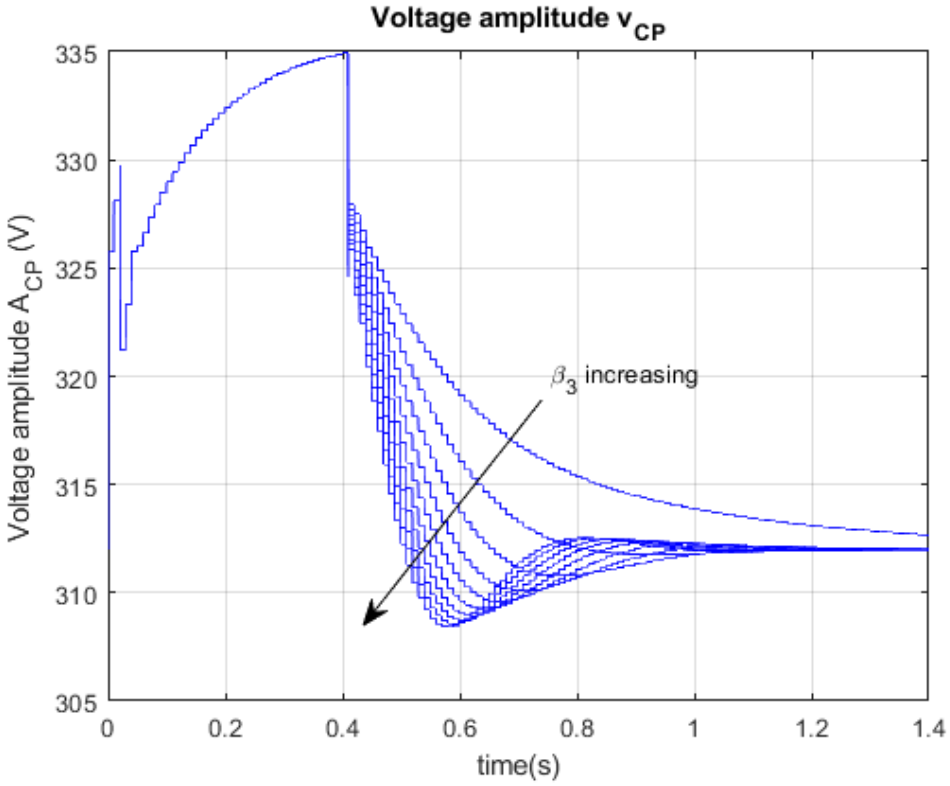

Figure 6.7: Voltage amplitude for real behavior changing β_3

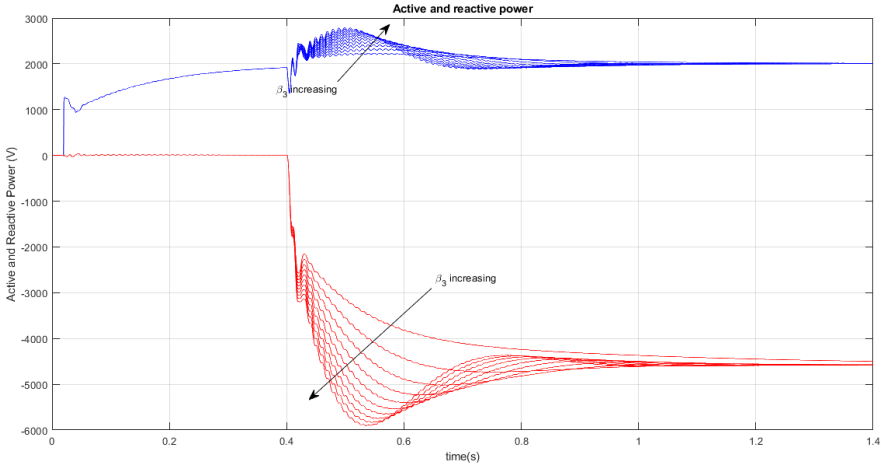

Figure 6.8: Active and reactive power for real behavior changing β_3

Below have been reported the pictures related to the root locus (Fig.6.9) the voltage amplitude (Fig.6.10) and active and reactive powers (Fig.6.11) for the Linearization method.

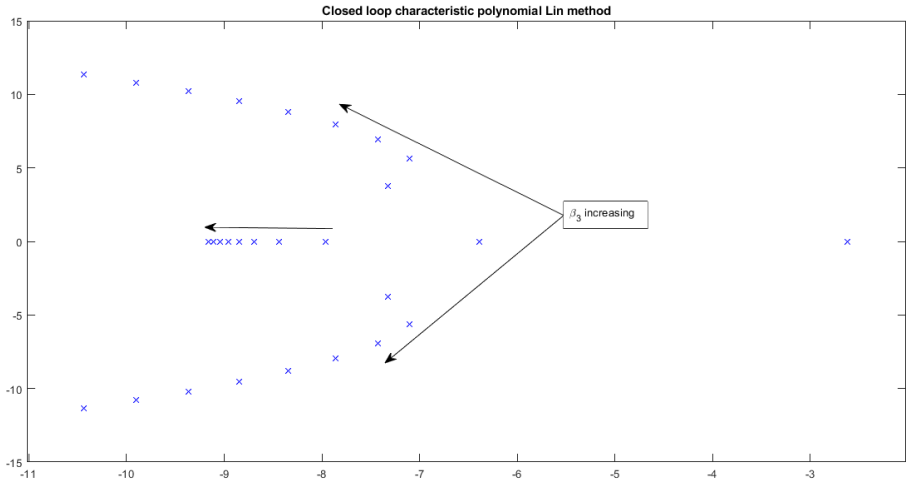

Figure 6.9: Root locus for Linearization method changing β_3

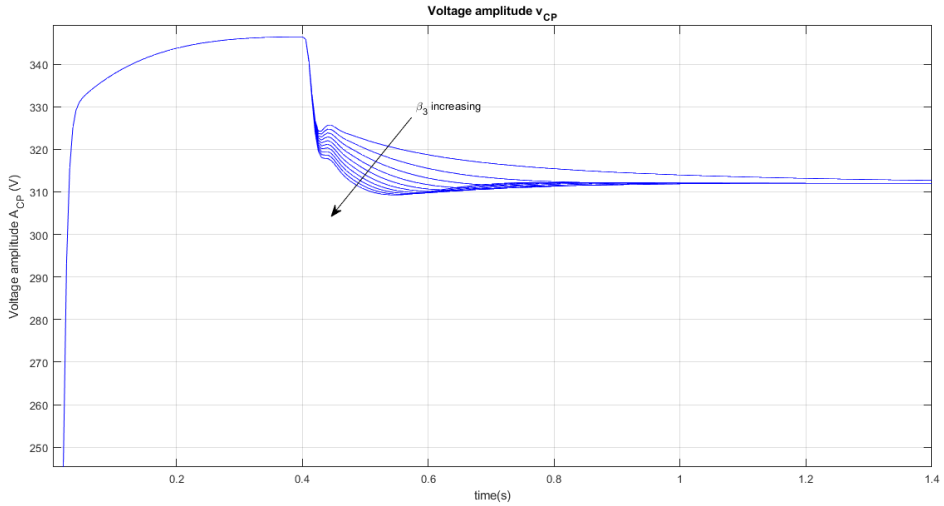

Figure 6.10: Voltage amplitude for Linearization method changing β_3

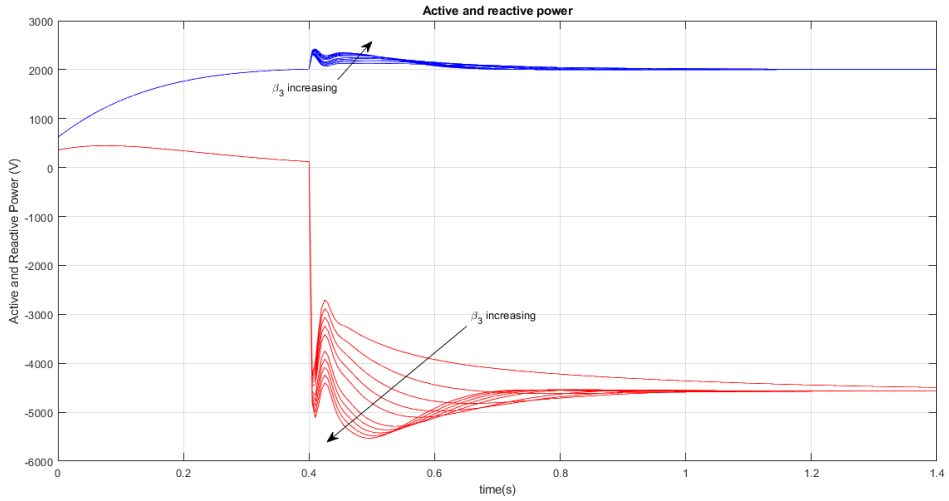

Figure 6.11: Active and reactive power for Linearization method changing β_3

Below have been reported the pictures related to the root locus (Fig.6.12) the voltage amplitude (Fig.6.13) and active and reactive powers (Fig.6.14) for the Drop method.

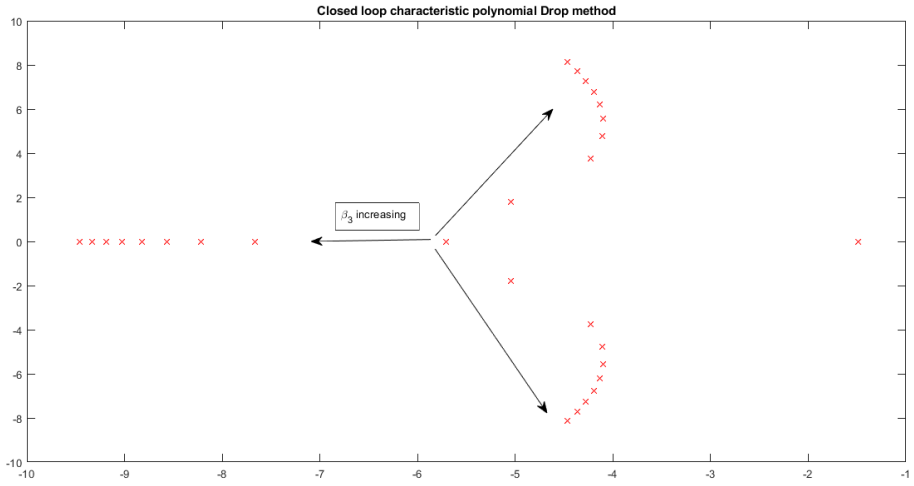

Figure 6.12: Root locus for Drop method changing β_3

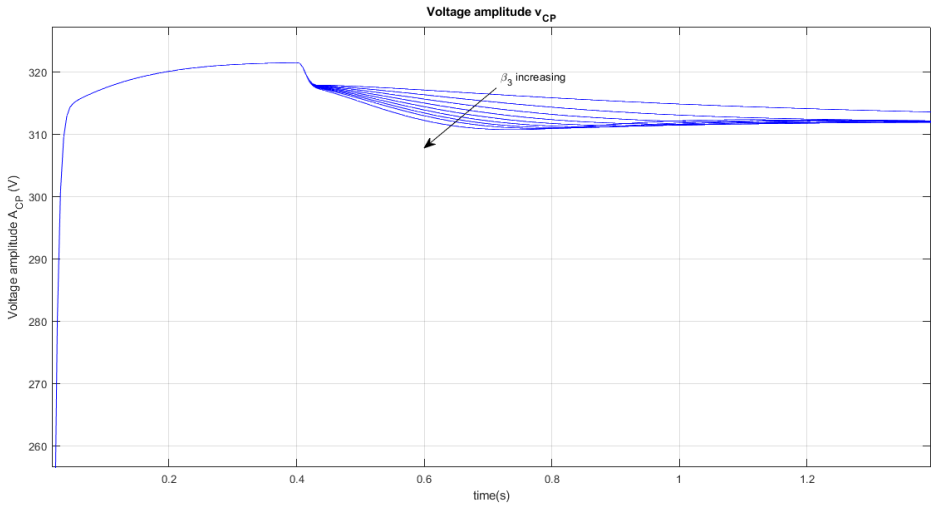

Figure 6.13: Voltage amplitude for Drop method changing β_3

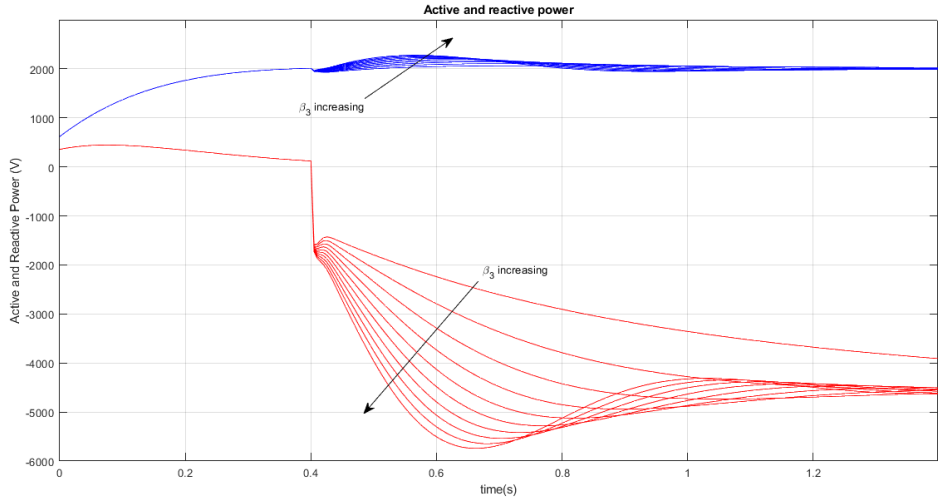

Figure 6.14: Active and reactive power for Drop method changing β_3

Chapter 7

Conclusions

This thesis evaluates different procedures for control design applied to regulate the amplitude of the voltage at the connection point in a PV inverter single-phase connected to a weakly grid. Usually this goal is achieved using PI controllers and this work compares two methods used to design the parameters of such PI controllers. This regulation is performed through a control loop that manages the output active and reactive power, as explained in the document. For this subject, the network has been considered to work at an equilibrium point, so fixing a reference values for the active and reactive power and obviously fixing the phase shift, in order to obtain at the connection point of the weakly grid the nominal voltage amplitude.
The methods compared here are: the Drop method and the Linearization method. The first one is very used nowadays, the other one is a more recent proposal. So, the main goal has been to demostrate what is the method that has trends closer to the real behavior.
Initially has been studied the problem statement, i.e. the variation of output impedance causes regulation problems for the voltage amplitude at connection point. The main problem appears when the output impedance has an inductive part, this introduces a necessary injection of reactive power. So the PF is not more equal to unity. Consequenty, the voltage amplitude at connection point is not equal to the nominal value. In this situation, the power control loop takes part and provides active and reactive power values in order to keep at the equilibrium point. Therefore, some sensitivity parameters has been included to characterize the dinamical behavior. This was the most important part of the comparison between both methods.
Through the development environment Matlab-Simulink has been possible to obtain the root locus graphs and to simulate the curves of powers and the curves of the voltage amplitude with the system parameters in order to prove analitically and demonstratively what is the "best method". Initially, the simulations have been done for a single case, where the output

impedance was fixed and all control parameters. Then, other simulations have been done changing a PI control parameter. The results obtained show that the Linearization method is better than other one because is closer to real behavior.

Bibliography

[1] M. A. Mahmud, M. J. Hossain, H. R. Pota and A. B. M. Nasiruzzaman, "Voltage control of distribution networks with distributed generation using reactive power compensation," *in Proc. 37th Annual Conference of the IEEE Industrial Electronics Society*, 2011.

[2] A. Molina-García, R. A. Mastromauro, T. Garcia-Sánchez, S. Pugliese, M. Liserre and S. Stasi, "Reactive Power Flow Control for PV Inverters Voltage Support in LV Distribution Networks," *in IEEE Transactions on Smart Grid*, Januray 2017.

[3] J. C. Vasquez, R. A. Mastromauro, J. M. Guerrero and M. Liserre, "Voltage Support Provided by a Droop-Controlled Multifunctional Inverter," *in IEEE Transactions on Industrial Electronics*, November 2009.

[4] E. Demirok, P. C. Gonzalez, K. H. B. Frederiksen, D. Sera, P. Rodriguez and R. Teodorescu, "Local Reactive Power Control Methods for Overvoltage Prevention of Distributed Solar Inverters in Low-Voltage Grids," *in IEEE Journal of Photovoltaics*, October 2011.

[5] A. Bonfiglio, M. Brignone, F. Delfino, R. Procopio, "Optimal Control and Operation of Grid-Connected Photovoltaic Production Units for Voltage Support in Medium-Voltage Networks," *in IEEE Transactions on Sustainable Energy*, January 2014.

[6] A. Cagnano, E. De Tuglie, M. Liserre, R.A. Mastromauro, "Online Optimal Reactive Power Control Strategy of PV Inverters," *in IEEE Transactions on Industrial Electronics*, October 2011.

[7] V.N. Lal, S.N. Singh, "Control and Performance Analysis of a Single-Stage Utility-Scale Grid-Connected PV System," *in IEEE Systems Journal*, in press.

[8] A. Anurag, Y. Yang, F. Blaabjerg, "Thermal Performance and Reliability Analysis of Single-Phase PV Inverters With Reactive Power Injection Outside Feed-In Operating Hours," *in IEEE Journal of Emerging and Selected Topics in Power Electronics*, December 2015.

[9] Y. Yang, H. Wang, F. Blaabjerg, "Reactive Power Injection Strategies for Single-Phase Photovoltaic Systems Considering Grid Requirements," *in IEEE Transactions on Industry Applications*, November-December 2014.

[10] Y. Yang, F. Blaabjerg, H. Wang, M.G. Simoes, "Power control flexibilities for grid-connected multi-functional photovoltaic inverters," *in IET Renewable Power Generation*, October 2016.

[11] R.I. Bojoi, L.R. Limongi, D. Roiu, A. Tenconi, "Enhanced Power Quality Control Strategy for Single-Phase Inverters in Distributed Generation Systems," *in IEEE Transactions on Power Electronics*, March 2011.

[12] W. Sripipat, S. Po-Ngam, "Simplified active power and reactive power control with MPPT for single-phase grid-connected photovoltaic inverters," *in Proc. Electrical Engineering/Electronics, Computer, Telecommunications and Information Technology*, 2014.

[13] Y. Yang, F. Blaabjerg, H. Wang, "Low-Voltage Ride-Through of Single-Phase Transformerless Photovoltaic Inverters," *in IEEE Transactions on Industry Applications*, May-June 2014.

[14] S. Dasgupta, S.K. Sahoo, S.K. Panda, "Single-Phase Inverter Control Techniques for Interfacing Renewable Energy Sources With Microgrid—Part I: Parallel-Connected Inverter Topology With Active and Reactive Power Flow Control Along With Grid Current Shaping," *in IEEE Transactions on Power Electronics*, March 2011.

[15] D. Biel, J.M.A. Scherpen, "Passivity-based control of active and reactive power in single-phase PV inverters," *in Proc. 26th IEEE International Symposium on Industrial Electronics*, June 2017.

[16] F. Marra et al., "EV Charging Facilities and Their Application in LV Feeders With Photovoltaics," *in IEEE Transactions on Smart Grid*, September 2013.

[17] M. Zeraati, M. E. Hamedani Golshan, J. M. Guerrero, "Distributed Control of Battery Energy Storage Systems for Voltage Regulation in Distribution Networks with High PV Penetration," *in IEEE Transactions on Smart Grid*, in press.

[18] N. Efkarpidis, T. De Rybel and J. Driesen, "Voltage regulation strategies for flemish LV distribution grids utilizing single-phase PV inverters," *in Proc. IEEE 6th International Symposium on Power Electronics for Distributed Generation Systems (PEDG)*, 2015.

[19] P. D. F. Ferreira, P. M. S. Carvalho, L. A. F. M. Ferreira and M. D. Ilic, "Distributed Energy Resources Integration Challenges in Low-Voltage Networks: Voltage Control Limitations and Risk of Cascading," *in IEEE Transactions on Sustainable Energy*, January 2013.

[20] R. Tonkoski, L. A. C. Lopes and T. H. M. El-Fouly, "Coordinated Active Power Curtailment of Grid Connected PV Inverters for Overvoltage Prevention," *in IEEE Transactions on Sustainable Energy*, April 2011.

[21] R. Ortega, J.A. Loira Perez, P.J. Nicklasson, H. Sira-Ramirez, *Passivity-based Control of Euler-Lagrange Systems*, Springer; 1998.

[22] C. Meza, D. Biel, D. Jeltsema, J.M.A. Scherpen. "Lyapunov-Based Control Scheme for Single-Phase Grid-Connected PV Central Inverters," *in IEEE Transactions on Control Systems Technology*, March 2012.

[23] D. del Puerto-Flores, J.M.A. Scherpen, M. Liserre, M.M.J. de Vries, M.J. Kransse, V.G. Monopoli, "Passivity-Based Control by Series/-Parallel Damping of Single-Phase PWM Voltage Source Converter," *in IEEE Transactions on Control Systems Technology*, July 2014.

[24] H. Komurcugil, "Steady-State Analysis and Passivity-Based Control of Single-Phase PWM Current-Source Inverters," *in IEEE Transactions on Industrial Electronics*, March 2010.

[25] J.J. Slotine, W. Li, *Applied Nonlinear Control*, Pearson Education; 1991.

[26] P. Chiradeja and R. Ramakumar, *An approach to quantify the technical benefits of distributed generation*, IEEE Trans. on Energy Conversion, vol. 19, no. 4, pp. 764–773, 2004.

[27] R. Kabiri, D. G. Holmes, B. P. McGrath and L. G. Meegahapola, "LV Grid Voltage Regulation Using Transformer Electronic Tap Changing, With PV Inverter Reactive Power Injection," *in IEEE Journal of Emerging and Selected Topics in Power Electronics*, December 2015.

[28] I. Diaz de Cerio Mendaza, I. G. Szczesny, J. R. Pillai and B. Bak-Jensen, "Demand Response Control in Low Voltage Grids for Technical and Commercial Aggregation Services," *in IEEE Transactions on Smart Grid*, November 2016.

[29] J. Machowski, J.W. Bialek, J.R. Bumby, *Power System Dynamics: Stability and Control*, John Wiley and Sons; 2008.

[30] B. Maschke, R. ortega, A.J. van der Schaft, "Energy-based Lyapunov functions for forced Hamiltonian systems with dissipation," *in IEEE Transactions on Automatic Control*, August 2000.

[31] A. Dell'Aquila, M. Liserre, V.G. Monopoli, C. Cecati, "Passivity-based control of a single-phase H-bridge multilevel active rectifier," *in Proc. IEEE Annual Conference of the Industrial Electronics Society*, 2002.

[32] A.F. Cupertino, J.T. de Resende, H.A. Pereira, S.I. Seleme Júnior, "A grid-connected photovoltaic system with a maximum power point tracker using passivity-based control applied in a boost converter," *in Proc. IEEE/IAS International Conference on Industry Applications*, 2012.

[33] D. Jeltsema, J.M.A. Scherpen. "Tuning of Passivity-Preserving Controllers for Switched-Mode Power Converters", *in IEEE Transactions on Automatic Control*, August 2004.

[34] Domingo Biel, Jacquelien M.A. Scherpen, "Active and reactive power regulation in single-phase PV inverters", *Proceedings of the European Control Conference 2018*, November 2018

[35] Domingo Biel, Jacquelien M.A. Scherpen, "Voltage regulation with power curtailment in a single-phase grid-connected PV inverter", *IEEE International Symposium on Circuits and Systems (ISCAS)*, May 2018.